

1           Significant source of secondary aerosol: formation from gasoline

2                    evaporative emissions in the presence of SO<sub>2</sub> and NH<sub>3</sub>

3           **Tianzeng Chen<sup>1,3,a</sup>, Yongchun Liu<sup>2,a</sup>, Qingxin Ma<sup>1,3,4,\*</sup>, Biwu Chu<sup>1,3,4</sup>, Peng Zhang<sup>1</sup>,**

4                               **Changgeng Liu<sup>1</sup>, Jun Liu<sup>1,3</sup>, Hong He<sup>1,3,4,\*</sup>**

5           <sup>1</sup> State Key Joint Laboratory of Environment Simulation and Pollution Control, Research Center for  
6           Eco-Environmental Sciences, Chinese Academy of Sciences, Beijing 100085, China

7           <sup>2</sup> Beijing Advanced Innovation center for Soft Matter Science and Engineering, Beijing University  
8           of Chemical Technology, Beijing 100029, China

9           <sup>3</sup> University of Chinese Academy of Sciences, Beijing 100049, China

10          <sup>4</sup> Center for Excellence in Regional Atmospheric Environment, Institute of Urban Environment,  
11          Chinese Academy of Sciences, Xiamen 361021, China

12          <sup>a</sup> These authors contributed equally to this work and should be considered as co-first authors

13          *Corresponding authors:* qxma@rcees.ac.cn (Qingxin Ma), and honghe@rcees.ac.cn (Hong He)

## 14 **Abstract**

15 Gasoline evaporative emissions have become an important anthropogenic source of urban  
16 atmospheric volatile organic compounds (VOCs) and secondary organic aerosol (SOA). These  
17 emissions have a significant impact on regional air quality, especially in China where car ownership  
18 is growing rapidly. However, the contribution of evaporative emissions on the secondary aerosol  
19 (SA) is not clear in air pollution complex in which high concentration of SO<sub>2</sub> and NH<sub>3</sub> was present.  
20 In this study, the effects of SO<sub>2</sub> and NH<sub>3</sub> on SA formation from unburned gasoline vapors were  
21 investigated in a 30 m<sup>3</sup> indoor smog chamber. It was found that increase in SO<sub>2</sub> and NH<sub>3</sub>  
22 concentrations (0–151 ppb and 0–200 ppb, respectively) could promote linearly the formation of  
23 SA, which could be enhanced by a factor of 1.6–2.6 and 2.0–2.5, respectively. Sulfate was most  
24 sensitive to the SO<sub>2</sub> concentration, followed by organic aerosol, which was due not only to the acid  
25 catalytic effect, but also related to the formation of organic sulfur-containing compounds. In the  
26 case of increasing NH<sub>3</sub> concentration, ammonium nitrate increased more significantly than organic  
27 aerosol, and nitrogen-containing organics were also enhanced, as revealed by the results of positive  
28 matrix factorization (PMF) analysis. New particle formation (NPF) and particle size growth were  
29 also significantly enhanced in the presence of SO<sub>2</sub> and NH<sub>3</sub>. This work indicates that gasoline  
30 evaporative emissions will be a significant source of SA, especially in the presence of high  
31 concentrations of SO<sub>2</sub> and NH<sub>3</sub>. Meanwhile, these emissions might also be a potential source of  
32 sulfur- and nitrogen-containing organics. Our work provides a scientific basis for the synergistic  
33 emission reduction of secondary aerosol precursors, including NO<sub>x</sub>, SO<sub>2</sub>, NH<sub>3</sub> and particularly  
34 VOCs, to mitigate PM pollution in China.

## 35 **Keywords**

36 Secondary inorganic aerosol; Secondary organic aerosol; Sulfur dioxide; Ammonia; Sulfur-

37 containing organics; Nitrogen-containing organics

## 38 **1 Introduction**

39 Many areas in China such as the Beijing - Tianjin - Hebei region (BTH), Yangtze River Delta (YRD),  
40 Sichuan Basin and Pearl River Delta (PRD) are suffering from severe haze events (Li et al., 2017; Sun et al.,  
41 2016; Shen et al., 2015; He et al., 2014; Huang et al., 2014; Guo et al., 2014; Tan et al., 2009). Haze pollution  
42 has attracted widespread attention in recent years because of its adverse effects on human health, climate  
43 change and visibility (Thalman et al., 2017; Davidson et al., 2005; Pöschl, 2005).

44 During the haze events, high concentrations of SO<sub>2</sub>, NH<sub>3</sub>, and volatile organic compounds (VOCs) have  
45 always been observed (Zou et al., 2015; Liu et al., 2013; Meng et al., 2011; Yang et al., 2009), which are the  
46 precursors of secondary aerosol. Although the emission of SO<sub>2</sub> has decreased continuously since 2005 (Lu  
47 et al., 2010), China is still the largest contributor of SO<sub>2</sub> emissions in the world, mainly owing to the great  
48 demand for coal combustion (Bauduin et al., 2016). Also, high concentrations of SO<sub>2</sub> of more than 100 ppb  
49 (parts per billion) have been observed in northern China, especially during the heating period (Hou et al.,  
50 2016; Tong et al., 2016; Yang et al., 2009). As for atmospheric NH<sub>3</sub>, as an alkaline inorganic gas, its main  
51 emission source is agricultural practices in China (Zhang et al., 2018; Fu et al., 2015). Vehicles equipped  
52 with three-way catalytic converters also contributes to NH<sub>3</sub> emission in the urban areas (Sun et al., 2017).  
53 Sometimes, high concentrations of NH<sub>3</sub> of up to 100 ppb have been observed in Beijing, China (Ianniello et  
54 al., 2010), which mainly derived from the regionally transportation of agricultural activity and fertilizer use,  
55 while could not exclude the influence by traffic emissions at local Beijing (Pan et al., 2016; Kang et al.,  
56 2016). With respect to VOCs, aromatics from anthropogenic sources (especially vehicle-related sources in  
57 urban areas) are critical secondary organic aerosol (SOA) precursors (Liu et al., 2015a; Gordon et al., 2014;  
58 Platt et al., 2013; Calvert et al., 2002). These aromatics could react with oxidants (e.g., O<sub>3</sub>, OH, and NO<sub>3</sub>  
59 radicals), and undergo multi-step oxidative processes to form multifunctional products, which have

60 sufficiently low volatility to contribute to SOA via gas-particle partitioning (Hallquist et al., 2009; Atkinson  
61 and Arey, 2003).

62 Researches have shown that secondary aerosol (SA) makes a significant contribution (30–77%) to  
63 PM<sub>2.5</sub> (particles with diameter less than 2.5 μm) during the severe haze events in China (Huang et al., 2014;  
64 Guo et al., 2014; Jimenez et al., 2009). However, there still exists a significant gap between the predicted  
65 SA derived from the current atmospheric quality models and that observed in field observations (Zhao et al.,  
66 2018; Yang et al., 2018; Zheng et al., 2015). Therefore, considering the characteristics of complex pollution  
67 in China, it is crucial to study the synergistic effects of SO<sub>2</sub> and NH<sub>3</sub> on the formation of SA, which have  
68 been considered an important potential source of SA formation (Zhao et al., 2018; Chu et al., 2016; Liu et  
69 al., 2016; Santiago et al., 2012; Na et al., 2007).

70 A few studies have focused on the influence of SO<sub>2</sub> or NH<sub>3</sub> on SA formation. Jang and Kamens (2001)  
71 first reported the acid-catalytical effect of acidic H<sub>2</sub>SO<sub>4</sub> on the oxidation of atmospheric carbonyls. And the  
72 promotion effect of SO<sub>2</sub> were further found on the SA formation from typical biogenic (e.g., isoprene and α-  
73 pinene) (Lin et al., 2013; Jaoui et al., 2008; Kleindienst et al., 2006; Edney et al., 2005) and anthropogenic  
74 (e.g., toluene, o-xylene, 1,3,5-trimethylbenzene, and gasoline vehicle exhaust) precursors (Chu et al., 2016;  
75 Liu et al., 2016; Santiago et al., 2012) through acid-catalyzed heterogeneous reactions (Jang et al., 2002;  
76 Jang et al., 2003a, b; Czoschke et al., 2003), which promote the reactive uptake process of organic species  
77 or enhance the formation of high-molecular-weight compounds (Liggio and Li, 2008; Liggio et al., 2007;  
78 Liggio and Li, 2006). With regard to the role of NH<sub>3</sub> in SA formation, knowledge is still limited. In previous  
79 studies, inconsistent impacts of NH<sub>3</sub> on SA formation have been reported under different precursor systems.  
80 For example, NH<sub>3</sub> could elevate SA formation in the α-pinene/ozone oxidation system through acid-base  
81 reactions (Na et al., 2007), while the effects of NH<sub>3</sub> neutralization were masked by other multiple factors

82 and did not show significant influence on isoprene-derived SOA formation (Lin et al., 2013), and addition  
83 of NH<sub>3</sub> even significantly reduced the SA formation in the styrene/ozone system, which was caused by  
84 nucleophilic attack from the NH<sub>3</sub> molecule leading to rapid decomposition of the major aerosol products (Na  
85 et al., 2006). For the photo-oxidation of aromatic VOCs (e.g., toluene, o-/m-/p-xylene), the presence of NH<sub>3</sub>  
86 could facilitate new particle formation (NPF) and particle growth, subsequently leading to increased SA  
87 formation (Li et al., 2018; Liu et al., 2015b).

88 At the present time, the effects of SO<sub>2</sub> and NH<sub>3</sub> on SA formation have rarely been studied under highly  
89 complex pollution conditions (Chu et al., 2016). Vehicular evaporative emissions have been reported to be  
90 non-negligible contributors (39.20 %) to ambient VOCs from anthropogenic sources compared with  
91 vehicular tailpipe emissions (Liu et al., 2017a). In addition to short-chain alkanes, a certain proportion of  
92 aromatics and alkanes (C<sub>6</sub> to C<sub>12</sub>) were also contained in the evaporative emissions (Liu et al., 2008; Zhang  
93 et al., 2013). Previous studies have reported that aromatics and long-chain (C<sub>6</sub> to C<sub>19</sub>) alkanes, which are  
94 intermediate volatility organic compounds (IVOCs) (Donahue et al., 2006), could contribute to SOA  
95 formation (Pye and Pouliot, 2012; Tkacik et al., 2012; Lim and Ziemann, 2005). Therefore, it is necessary  
96 to study the influence of SO<sub>2</sub> and NH<sub>3</sub> on SA formation from evaporative emissions.

97 In this study, unburned gasoline vapors were used as a substitute for evaporative emissions, and the  
98 roles of SO<sub>2</sub> and NH<sub>3</sub> on SA formation from the photo-oxidation of unburned gasoline vapors were  
99 investigated in a 30 m<sup>3</sup> indoor smog chamber, in order to understand the formation potential of SA from  
100 oxidation of gasoline vapor in the cocktail of pollutants in Beijing. The respective influences of SO<sub>2</sub> and  
101 NH<sub>3</sub> on both the microphysics and chemistry of SA formation were examined. Meanwhile, the chemical  
102 compositions of the formed SOA in the presence of SO<sub>2</sub> and NH<sub>3</sub> were further explored by applying positive  
103 matrix factorization (PMF) analysis. The formation potentials of SA, sulfur- and nitrogen-containing

104 organics from vehicular evaporative emissions in the presence of SO<sub>2</sub> and NH<sub>3</sub> were evaluated and discussed.

## 105 **2 Materials and Methods**

### 106 **2.1 Gasoline fuel**

107 The utilized gasoline fuel with grade 92# was collected (refer to the standard Method for manual  
108 sampling of petroleum liquids (GB/T 4756-2015)) from a gas station located in Beijing. The gasoline  
109 complies with the China V gasoline fuel standard. It contains 65.1 % (v/v) alkanes (C6 to C12), 22.8 % (v/v)  
110 aromatics (mainly including benzene, toluene, xylene, trimethylbenzene) and 12.1 % (v/v) alkenes. The  
111 composition of the gasoline is similar to the gasoline collected in North China reported by Tang et al. (2015)  
112 and could represent the gasoline used in most areas of China for studying SA formation potential. Details of  
113 the gasoline composition are given in Table S1.

### 114 **2.2 Smog chamber facility**

115 A series of photochemical experiments with unburned gasoline vapors in the absence or presence of  
116 SO<sub>2</sub> or NH<sub>3</sub> were performed in a 30 m<sup>3</sup> indoor smog chamber at the Research Center for Eco-Environmental  
117 Sciences, Chinese Academy of Sciences (RCEES-CAS). The detailed schematic structure of the indoor smog  
118 chamber is given in Fig. S1 in the Supplement and described elsewhere (Chen et al., 2019a, b). Briefly, the  
119 cuboid chamber reactor ( $L \times W \times H = 3.0 \times 2.5 \times 4.0$  m,  $S/V = 1.97$  m<sup>-1</sup>) was irradiated by 120 UV lamps  
120 (Philips) with peak intensity at 365 nm, providing a NO<sub>2</sub> photolysis rate of 0.55 min<sup>-1</sup>. The interior was  
121 coated with 125 μm-thick FEP100 film (DuPont™, US) and the chamber was located in a temperature-  
122 controlled room, in which the temperature (T) and relative humidity (RH) could be controlled mechanically.  
123 A three-wing stainless-steel fan coated with Teflon was installed inside the reactor to guarantee that the gas  
124 and particle phase species mix sufficiently before photochemical reaction.

125 The chamber was also equipped with a series of gas- and particle-phase monitoring instruments. For

126 gaseous NO<sub>x</sub>, O<sub>3</sub> and SO<sub>2</sub>, a chemiluminescence analyzer (Model 42i-TL, Thermo Fisher Scientific, USA),  
127 a UV photometric analyzer (Model 49i, Thermo Fisher Scientific, USA) and a pulsed fluorescence analyzer  
128 (Model 43i, Thermo Fisher Scientific, USA) were used to monitor the concentrations in real time,  
129 respectively. The VOC species in gasoline were measured with a gas chromatograph (7890B GC, Agilent,  
130 USA) equipped with a DB-624 column (60 m × 0.25 mm × 1.40 μm, Agilent, USA) and a mass spectrometry  
131 detector (5977A MS, Agilent, USA) (GC-MS). In addition, proton-transfer-reaction time of flight mass  
132 spectrometry (PTR-TOF) (Ionicon Analytik GmbH, Austria) was also used for the measurement of gas-  
133 phase hydrocarbons and their intermediate products (Yuan et al., 2017). The size distribution and number  
134 concentration of the formed particulate matter (PM) were measured using a scanning mobility particle sizer  
135 (SMPS, TSI, USA), which was composed of a differential mobility analyzer (DMA, 3080 Classifier, TSI,  
136 USA) coupled with a condensation particle counter (CPC, 3776, TSI, USA). The mass concentration was  
137 estimated based on the volume concentration and the density of PM calculated from the equation  $\rho = d_{va}/d_m$ ,  
138 where  $d_{va}$  is the mean vacuum aerodynamic diameter measured by an Aerodyne high-resolution time-of-  
139 flight aerosol mass spectrometer (HR-ToF-AMS) and  $d_m$  is the mean electrical mobility diameter measured  
140 by SMPS (DeCarlo et al., 2004). The calculated density of PM ranged from 1.5 to 1.6 g cm<sup>-3</sup> in the different  
141 reaction systems, which was in the range of density of SOA derived from aromatic hydrocarbons (1.24–1.48  
142 g cm<sup>-3</sup>) (Sato et al., 2010) and ammonium nitrate (NH<sub>4</sub>NO<sub>3</sub>, 1.72 g cm<sup>-3</sup>) (Bahreini et al., 2005) and could  
143 be comparable with the previous studies (Li et al., 2018). The mass concentration and chemical composition  
144 of PM were simultaneously monitored using a high-resolution time-of-flight aerosol mass spectrometer (HR-  
145 ToF-AMS, Aerodyne Research Inc. USA). For all experiments, the HR-ToF-AMS operated in a cycle  
146 including two modes, 3 min V mode and 2 min W mode. Specifically, V mode (higher signal) can obtain the  
147 mass concentrations of the aerosols and W mode (higher resolution) can obtain high resolution mass spectral



148 data. The inlet flow rate, ionization efficiency (IE), and particle sizing were calibrated according to the  
149 standard protocols (Drewnick et al., 2005; Jimenez et al., 2003; Jayne et al., 2000), using the size-selected  
150 pure ammonium nitrate (AN) particles. All HR-ToF-AMS data were analyzed with ToF-AMS analysis  
151 toolkit SQUIRREL 1.57I/PIKA 1.16I version, in Igor Pro Version 6.37. HR-ToF-AMS results were also  
152 corrected using the mass concentration derived from SMPS according to the same method as Gordon et al.  
153 (2014), details of this correction are shown in the Supplement. As for the RH control system, it is achieved  
154 by vaporizing Milli-Q ultrapure water contained in a 5.0 L high pressure resistant container and the water  
155 vapor is flushed with purified dry zero air into the chamber. T and RH were monitored real-time using a  
156 hydro-thermometer (Vaisala HMP110) during the entirety of each experiment.

### 157 **2.3 Wall loss corrections**

158 The measured particle concentration was corrected in accordance with the relationship between the  
159 deposition rate ( $k_{\text{dep}}$ ) and particle diameter ( $D_p$ , nm) (i.e.,  $k_{\text{dep}} = 4.15 \times 10^{-7} \times D_p^{1.89} + 1.39 \times D_p^{-0.88}$ ), which  
160 was described by Takekawa et al. (2003). The wall loss rates of NO<sub>2</sub>, NO, O<sub>3</sub>, SO<sub>2</sub> and VOC species were  
161 determined to be  $(1.67 \pm 0.25) \times 10^{-4}$ ,  $(1.32 \pm 0.32) \times 10^{-4}$ ,  $(3.32 \pm 0.21) \times 10^{-4}$ ,  $(4.52 \pm 0.11) \times 10^{-4}$  and  $(2.20$   
162  $\pm 0.39) \times 10^{-4} \text{ min}^{-1}$ , respectively. Therefore, the wall loss of gas phase species was evaluated to be less than  
163 5% of their maximum concentration in this study.

164 Wall losses of semi-volatile organic compounds (SVOCs) and low-volatility organic compounds  
165 (LVOCs) would lead to a substantial underestimation of SA formation (Krechmer et al., 2016; Ye et al., 2016;  
166 Zhang et al., 2015; Zhang et al., 2014), which is caused by the competition between these vapors condensing  
167 onto particles versus onto chamber walls. This competition could be evaluated by the corresponding  
168 timescales associated with reaching gas-to-particle partitioning equilibrium ( $\bar{\tau}_{\text{g-p}}$ ) and vapor wall loss ( $\tau_{\text{g-w}}$ )  
169 (Zhang et al., 2014), and this underestimation of SA formation could be approximately quantified by the

170 ratio of these two timescales (i.e.,  $\bar{\tau}_{g-p}/\tau_{g-w}$ ). According to the methods described by Zhang et al. (2014),  $\bar{\tau}_{g-}$   
171  $p$  and  $\tau_{g-w}$  could be estimated assuming an upper bound and a lower bound of the molecular mass of organic  
172 vapors (MW) (100–300 g mol<sup>-1</sup>) (as discussed in the Supplement). In order to accurately quantify the SA  
173 formation, the underestimation caused by the loss of SVOCs and LVOCs (include sulfuric acid gas) to the  
174 chamber walls was taken into account in this study. In this study, the SA yields were underestimated by a  
175 factor of 1.97–2.82 fold when considering the ratio of these two timescales (i.e.,  $\bar{\tau}_{g-p}/\tau_{g-w}$ ), which showed a  
176 decreasing trend with the increase of the SO<sub>2</sub> and NH<sub>3</sub> initial concentrations, suggesting that an increasing  
177 proportion of vapors is partitioned onto the suspended particle surface rather than the chamber wall.

## 178 **2.4 Experimental conditions**

179 Prior to each experiment, the chamber reactor was flushed by purified and dry zero air for about 24–36  
180 h at a flow rate of 100 L min<sup>-1</sup> until almost no gas-phase species (i.e., NO<sub>x</sub>, O<sub>3</sub> and SO<sub>2</sub>) could be detected  
181 (< 1 ppb) and the particle number concentration was < 10 cm<sup>-3</sup>. Before the experiments, the chamber was  
182 humidified to ~50 % RH by passing purified zero air through ultra-pure water (18.2 MΩ, Millipore Milli-  
183 Q). After that, a known volume of liquid gasoline (100 μL) was injected into the chamber through a heated  
184 Teflon line system (~100 °C) carried by purified dry zero air to ensure that all were evaporated into the  
185 chamber. Subsequently, NO, SO<sub>2</sub> or/and NH<sub>3</sub> were successively injected into the chamber from standard gas  
186 cylinders using mass flow controllers. The initial VOCs/NO<sub>x</sub> ratio (ppbC ppb<sup>-1</sup>) was kept constant (Table 1).  
187 In order to reduce the adsorption of NH<sub>3</sub> in the pipeline, the NH<sub>3</sub> flow in a bypass line was balanced for  
188 about 30 min before it was injected into the chamber. The concentrations of NO and SO<sub>2</sub> were continuously  
189 monitored until they were stable, ensuring that the gaseous species mixed well in the chamber. For the  
190 concentration of NH<sub>3</sub>, the value was estimated according to the amount of NH<sub>3</sub> introduced and the volume  
191 of the reactor chamber. The experiment was then conducted for about 8 h after turning off the fan and turning

192 on the UV lights. All the experiments were performed at a temperature of  $26 \pm 1$  °C and wet conditions (RH  
193 =  $50 \pm 3$  %). The detailed experimental conditions are listed in Table 1. The letters in the abbreviations  
194 represent the reactants introduced into the chamber reactor for each experiment. For example, SGN is an  
195 experiment with the presence of sulfur dioxide (S), gasoline vapor (G), and nitrogen oxides (N). Four  
196 experiments (Exps. SGN1, SGN2, SGN3, and SGN4) were carried out at different SO<sub>2</sub> initial concentrations.  
197 AGN is an experiment with the presence of ammonia (A), gasoline vapor (G), and nitrogen oxides (N). Two  
198 experiments (Exps. AGN1 and AGN2) were carried out at different NH<sub>3</sub> initial concentrations.

### 199 **3 Results and discussion**

#### 200 **3.1 Effect of SO<sub>2</sub> and NH<sub>3</sub> on the gas-phase species**

201 Time-resolved concentrations of inorganic and organic gas-phase species during the photo-oxidation of  
202 gasoline/NO<sub>x</sub> in the absence or presence of SO<sub>2</sub> and NH<sub>3</sub> are shown in Fig. S2 and Fig. S3 in the Supplement,  
203 respectively. After turning on the UV lights, NO was rapidly converted to NO<sub>2</sub>. At the same time, O<sub>3</sub> was  
204 gradually generated, with a maximum concentration of up to 350 ppb (Fig. S2). As shown in Fig. S2, there  
205 was no obvious difference in the variation of NO<sub>x</sub> and O<sub>3</sub> in the presence of SO<sub>2</sub> or NH<sub>3</sub>. Additionally, the  
206 decay of typical VOC precursors (e.g., benzene, toluene, methylcyclopentane, methylcyclohexane)  
207 measured by PTR-TOF and GC-MS are given in Fig. S3, which traced very closely with each other (Fig. S4,  
208 in the Supplement). There were also no observable differences in these precursors VOCs among these  
209 experiments. According to the decay curves of aromatic hydrocarbons, the OH radical concentrations were  
210 estimated to be  $(7.54\text{--}8.40) \times 10^6$  molecules cm<sup>-3</sup>, which were also similar among these experiments. This  
211 was consistent with the previous study conducted by Chu et al. (2016), who found that the presence of SO<sub>2</sub>  
212 and NH<sub>3</sub> did not significantly impact the OH concentration during the photo-oxidation of toluene in the  
213 presence of NO<sub>x</sub>.

214 However, as for the gas-phase intermediates formed during the photo-oxidation of gasoline/NO<sub>x</sub> under  
215 different conditions, such as small molecule oxygenated VOCs (OVOCs), which could also be measured by  
216 PTR-TOF. The time series of OVOCs concentration would vary with the concentration of SO<sub>2</sub> and NH<sub>3</sub>. For  
217 example, we observed that acetic acid concentration decreased with the increased concentration of SO<sub>2</sub> (Fig.  
218 S5, in the Supplement), suggesting that the uptake of acetic acid may be enhanced. This phenomenon was  
219 consistent with those reported by Liggio and Li (2006), who observed that the uptake of organic compounds  
220 under acidic conditions would be enhanced significantly. Moreover, the presence of high concentrations of  
221 SO<sub>2</sub> would generate gaseous H<sub>2</sub>SO<sub>4</sub>, which would contribute to the formation of particle phase, as discussed  
222 in the next section. Similarly, the concentration of acetic acid also shown an obviously decreased trend in  
223 the presence of NH<sub>3</sub> (Fig. S5, in the Supplement), which could be caused by the reaction of acid-base reaction  
224 or the uptake of acetic acid in the presence of NH<sub>3</sub> (Liu et al., 2015c).

### 225 **3.2 Role of SO<sub>2</sub> in secondary aerosol formation**

226 To investigate the effects of SO<sub>2</sub> on SA formation from the photo-oxidation of gasoline/NO<sub>x</sub>, smog  
227 chamber experiments with different SO<sub>2</sub> initial concentrations were carried out (Table 1). As shown in Fig.  
228 1, compared to the experiments without the addition of SO<sub>2</sub>, the SA concentration was enhanced to different  
229 degrees (1.6–2.6 times) in the presence of different SO<sub>2</sub> concentrations (35–151 ppb, i.e., 100–431 μg m<sup>-3</sup>).  
230 As for each chemical species (i.e., organics, nitrate, sulfate, and ammonium), they all showed a trend of  
231 linear increase with the increase of SO<sub>2</sub> concentration (Fig. 2), especially for the sulfate ( $k = 8.4 \times 10^{-2}$ ) and  
232 organic aerosol ( $k = 2.9 \times 10^{-2}$ ). Previous studies have also revealed its promoting role on SA formation from  
233 different precursors (Zhao et al., 2018; Liu et al., 2017b; Díaz-de-Mera et al., 2017; Liu et al., 2016; Chu et  
234 al., 2016).

235 Additionally, the particle number concentrations and size growth were greatly enhanced by the presence

236 of SO<sub>2</sub>. As evident from Fig. 3, the corresponding maximal particle number concentrations ( $5.82 \times 10^4$ – $1.91$   
237  $\times 10^5$  cm<sup>-3</sup>) were significantly enhanced by a factor of 2.9–3.3 in the presence of SO<sub>2</sub>. This universal  
238 phenomenon has been reported by many studies (Díaz-de-Mera et al., 2017; Liu et al., 2017b; Liu et al.,  
239 2016; Chu et al., 2016). For example, the maximal particle number concentrations were enhanced by the  
240 presence of SO<sub>2</sub> (~130 ppb) to one order of magnitude in the photo-oxidation of high concentration  
241 toluene/NO<sub>x</sub> (Chu et al., 2016). For complex precursor systems (gasoline vehicle exhaust), Liu et al. (2016)  
242 have also found that under high SO<sub>2</sub> concentration (~150 ppb) conditions, the maximum particle number  
243 concentrations increased by 5.4–48 times compared to those without SO<sub>2</sub> during the photo-oxidation of  
244 gasoline vehicle exhaust. This higher magnification of SO<sub>2</sub> might be related to the different VOCs  
245 composition between evaporative emissions and gasoline vehicle exhaust, especially the aromatic and  
246 IVOCs (Liu et al., 2017). Our recent study demonstrated that SOA formation could be significantly enhanced  
247 by the increase of aromatic content (Chen et al., 2019b). Those unspciated organic emissions (e.g., IVOCs)  
248 from gasoline vehicle exhaust would also have a significant contribution to SOA formation (Jathar et al.,  
249 2014; Gordon et al., 2014). Moreover, a small amount of POA was present in the initial reaction systems in  
250 Liu et al. (2016). These enhanced SOA formation and the pre-existing POA would provide larger surface  
251 areas for the condensation and heterogeneous uptake of low-volatility vapors (e.g., gaseous H<sub>2</sub>SO<sub>4</sub>), then  
252 promoting a higher magnification in particle number concentrations in the presence of SO<sub>2</sub>. The higher initial  
253 mixing ratios of precursors (2.2–4.3 ppm) was also present in the reaction systems conducted by Liu et al.  
254 (2016), which would further be beneficial to the SOA formation. In addition, size distributions of generated  
255 SA in smaller size ranges (4–160 nm) were also determined using another SMPS equipped with a nanometer  
256 differential mobility analyzer (Nano-DMA), indicating that the new particle formation (NPF) phenomenon  
257 was enhanced significantly when the SO<sub>2</sub> concentration increased (Fig. S6). The presence of high

258 concentrations of SO<sub>2</sub> would generate sulfuric acid (H<sub>2</sub>SO<sub>4</sub>), which would contribute to nucleation and  
259 increase the total particle number concentrations (Zhao et al., 2018; Sipilä et al., 2010). As the SO<sub>2</sub>  
260 concentration increased from 35 ppb to 151 ppb, the maximal particle diameters (144–172 nm) became  
261 larger, which will have a direct impact on the scattering and absorption of light (Seinfeld and Pandis, 2016).  
262 An enhancement effect of SO<sub>2</sub> on the surface area of particles was also observed. As shown in Table 1, the  
263 surface area of aerosol particles at the end of each experiment increased from  $1.12 \times 10^3$  to  $2.46 \times 10^3 \mu\text{m}^2$   
264  $\text{cm}^{-3}$  when the SO<sub>2</sub> concentration increased from 0 to 151 ppb. The larger surface area would be beneficial  
265 to the condensation and heterogeneous uptake of low-volatility vapors (Chapleski et al., 2016), consequently  
266 leading to higher SA yield in the presence of SO<sub>2</sub> (Table 1) (Santiago et al., 2012). Additionally, it is worth  
267 noting that there was a discrepancy between the magnification of particle number concentrations, surface  
268 areas and SO<sub>2</sub> concentrations. On one hand, there might be some particles, especially nanoclusters, were lost  
269 to the chamber wall and not be detected; on the other hand, the initial size of nanoclusters contributed from  
270 gaseous H<sub>2</sub>SO<sub>4</sub> was small enough (sub-3 nm) (Chu et al., 2019; Sipilä et al., 2010) and couldn't be detected  
271 by our general SMPS. That is to say, the particle number concentrations and surface areas measured by our  
272 SMPS might be the particles after growing up by collision. This could be supported by the enhancement in  
273 the particle diameters (144–172 nm) and sulfate concentrations ( $13\text{--}38 \mu\text{g m}^{-3}$ ) in the presence of SO<sub>2</sub>. After  
274 considering the underestimation of particles formation (factor of 1.97–2.82, seen in Section 2.3), the sulfate  
275 concentrations will be enhanced by a factor of 5.8 when comparing between experiments SGN 1 and SGN  
276 4.

277 In order to further investigate the role of SO<sub>2</sub> in the chemistry of SOA formation, the particle acidities  
278 were estimated using the E-AIM model (Model II: H<sup>+</sup> - NH<sub>4</sub><sup>+</sup> - SO<sub>4</sub><sup>2-</sup> - NO<sub>3</sub><sup>-</sup> - H<sub>2</sub>O) (Clegg and Brimblecombe,  
279 2005; Wexler and Clegg, 2002; Clegg et al., 1998). The concentrations of chemical components (i.e., NH<sub>4</sub><sup>+</sup>,

280  $\text{SO}_4^{2-}$ , and  $\text{NO}_3^-$ ) at the time when the SOA formation rate reached its peak were used as the inputs of the  
281 model. As shown in Fig. 4, the  $\text{H}^+$  concentration was increased from 8.5 to 32.5  $\text{nmol m}^{-3}$  with the increase  
282 of  $\text{SO}_2$  concentration under moderate humidity conditions ( $\text{RH} = 50\%$ ) and the higher SOA concentration  
283 and SOA yield could be well explained by the enhancement of the particle acidities ( $R^2 = 0.960$  and  $R^2 =$   
284  $0.986$ , respectively). The higher SOA concentration and SOA yield were related to the acid-catalyzed  
285 reactions of multifunctional aldehydes (e.g., glyoxal and methylglyoxal), which were the products of  
286 aromatic hydrocarbons in the gasoline vapors through the gas-phase photo-oxidation. Hemiacetals, acetals  
287 and alcohols could be generated through the acid-catalyzed heterogeneous reactions of glyoxal (Czoschke  
288 et al., 2003; Jang et al., 2002). These low-vapor-pressure products generated from heterogeneous reactions  
289 preferentially contribute to the SOA formation (Kroll and Seinfeld, 2008; Cao and Jang, 2007; Casale et al.,  
290 2007; Jang et al., 2002).

291 In addition, the sulfur-containing organics formed in the presence of  $\text{SO}_2$  might be another reason for  
292 the increase of SOA yield (Kundu et al., 2013; Liggio et al., 2005). Jaoui et al. (2008) have reported that the  
293 acidic aerosol generated in the presence of  $\text{SO}_2$  could lead to sulfur-incorporating reactions in the particle  
294 phase during the photo-oxidation of  $\alpha$ -pinene/toluene/ $\text{NO}_x$  mixtures. Sulfur-containing organics could be  
295 generated via reactions of organic species (e.g., polycyclic aromatic hydrocarbons (PAHs), C10–C12 alkanes,  
296 alcohols, epoxides) with sulfate, bisulfate or sulfuric acid, especially under high relative humidity and acidity  
297 conditions (Riva et al., 2015, 2016; Huang et al., 2015; Hatch et al., 2011; Surratt et al., 2007; Liggio et al.,  
298 2005). Huang et al. (2015) have revealed that sulfur-containing organics with R-O- $\text{SO}_3^-$  functional groups  
299 will yield S-bearing organic fragments ( $\text{C}_x\text{H}_y\text{O}_z\text{S}$ ) during ionization, which subsequently could be detected  
300 by HR-ToF-AMS and used as marker ions to quantify them. In our gasoline/ $\text{NO}_x$  experiments in the presence  
301 of  $\text{SO}_2$ , the ions  $\text{CSO}^+$ ,  $\text{CH}_3\text{SO}_2^+$  and  $\text{CH}_3\text{SO}_3^+$  could be separated (Fig. S7), although uncertainty might be

302 induced in the peak-fitting of the highly abundant ions  $C_2H_4O_2^+$ ,  $C_6H_7^+$ , and  $C_5H_3O_2^+$ . These characteristic  
303 ions (i.e.,  $CSO^+$ ,  $CH_3SO_2^+$  and  $CH_3SO_3^+$ ) also have been observed from sulfur-containing organics in  
304 previous field measurements (Huang et al., 2015; Farmer et al., 2010). According to the estimation method  
305 for sulfur-containing organics mentioned in Huang et al. (2015), we found that the signal of these ions and  
306 the concentrations of sulfur-containing organics increased with the  $SO_2$  initial concentration (Fig. 5). The  
307 conservative lower-bound estimated concentrations of sulfur-containing organics ( $13\text{--}26\text{ ng m}^{-3}$ ) were  
308 comparable to those ( $\sim 20\text{ ng m}^{-3}$ ) observed in the mid-Atlantic United States, which were derived from  
309 biogenic and anthropogenic hydrocarbons (Meade et al., 2016). Additionally, it should be noted that the  
310 sulfur-containing organics concentration in this study might be underestimated by the HR-ToF-AMS when  
311 considering one cannot resolve all the sulfur-containing fragments that may exist, and some of the sulfur-  
312 containing organics might fragment into masses that do not contain sulfur and thus are quantified as organic.  
313 Furthermore, the relative ionization efficiency (RIE) for the sulfur-containing organics fragments was  
314 assumed to be equivalent to the remainder of the organics (1.3), since a RIE value for sulfur-containing  
315 organics is unknown. This may introduce an additional uncertainty to the quantitation of sulfur-containing  
316 organics. Therefore, photo-oxidation of gasoline vapor in the presence of  $SO_2$  might be a noteworthy source  
317 of sulfur-containing organics, although the concentration was very low compared to that of generated  $SO_4^{2-}$   
318 ( $\sim 0.1\%$  of  $SO_4^{2-}$ ).

### 319 **3.3 Role of $NH_3$ in secondary aerosol formation**

320 Similarly, the role of  $NH_3$  in SA formation was examined. It is worth noting that ammonium aerosols  
321 were formed without the addition of gaseous  $NH_3$  (Fig. S8, in the Supplement), which signified that some  
322  $NH_3$  was present in the background air in the chamber or introduced during the humidification process of  
323 the chamber (Liu et al., 2015c). Unfortunately, appropriate instruments are unavailable to measure the exact



324 concentration of background  $\text{NH}_3$  in the chamber. According to the concentration of generated ammonium  
325 aerosols, the concentration of background  $\text{NH}_3$  was estimated to be  $\sim 15$  ppb using the E-AIM model (Clegg  
326 and Brimblecombe, 2005; Wexler and Clegg, 2002; Clegg et al., 1998). Therefore, for the experiments with  
327 the presence of  $\text{NH}_3$ , the concentration of injected  $\text{NH}_3$  (150–200 ppb) was much higher than this value to  
328 identify the effect of  $\text{NH}_3$  on SA formation. The SA concentration was enhanced by a factor of 2.0–2.5 in  
329 the presence of  $\text{NH}_3$ , as shown in Fig. S9a. The formation of SOA,  $\text{NO}_3^-$  and  $\text{NH}_4^+$  was enhanced to varying  
330 degrees. The increase of  $\text{NO}_3^-$  and  $\text{NH}_4^+$  could be attributed to the formation of inorganic  $\text{NH}_4\text{NO}_3$  in the  
331 presence of  $\text{NH}_3$ . The  $\text{NO}^+/\text{NO}_2^+$  ratio, which could be derived from HR-ToF-AMS, has often been used as  
332 a proxy for identification of inorganic nitrate and organic nitrogen compounds (Farmer et al., 2010; Sato et  
333 al., 2010; Rollins et al., 2009). Generally, the  $\text{NO}^+/\text{NO}_2^+$  ratio of inorganic nitrate (1.08–2.81) is lower than  
334 that of organic nitrogen compounds (3.82–5.84) (Liu et al., 2016). In this study, the  $\text{NO}^+/\text{NO}_2^+$  ratio became  
335 substantially lower ( $\sim 2.00$ ) in the presence of  $\text{NH}_3$  compared with that in the absence of  $\text{NH}_3$  ( $\sim 5.46$ ).  
336 Therefore,  $\text{NH}_4\text{NO}_3$  was the dominant nitrate species in the presence of  $\text{NH}_3$ . As for the reason for SOA  
337 enhancement, the presence of  $\text{NH}_3$  could react with some organic acids and subsequently contribute to SOA  
338 formation (Na et al., 2007; Na et al., 2006), which could be supported by the increase of N/C (from 0.016 to  
339 0.033) with increasing  $\text{NH}_3$  concentration at similar concentrations of  $\text{NO}_x$ . In addition, we have found that  
340 the presence of  $\text{NH}_3$  readily increased the particle diameter and number concentration of SA generated in the  
341 photo-oxidation of gasoline (Figs. S9b and S9c), which revealed that  $\text{NH}_3$  played an important role in new  
342 particle formation (NPF). These are consistent with the simulation results finding that  $\text{NH}_3$  promotes  
343 atmospheric NPF and also the conversion of  $\text{SO}_2$  and  $\text{NO}_2$  (Jiang and Xia, 2017). The increased surface area  
344 of particles was also observed (Table 1,  $2.07 \times 10^3$  and  $2.48 \times 10^3 \mu\text{m}^2 \text{cm}^{-3}$ ) as the  $\text{NH}_3$  concentration  
345 increased from 0 to 150 and 200 ppb. Similarly, the larger surface area would favor the partitioning of low-

346 volatility vapors to the particle phase, leading to the higher SA yield (Table 1).

347 Previous studies have reported that the reaction of carbonyl compounds (e.g., glyoxal) could be  
348 catalyzed by  $\text{NH}_4^+$  ions through a Bronsted acid pathway or an iminium pathway, which could generate N-  
349 containing products and oligomers (Nozière et al., 2009), and then contribute a substantial fraction to SOA  
350 (Liu et al., 2015c; Farmer et al., 2010; Cheng et al., 2006). Researchers have identified the characteristic  
351 fragments of nitrogen-containing organics as  $\text{C}_x\text{H}_y\text{N}_n$  and  $\text{C}_x\text{H}_y\text{O}_z\text{N}_n$  using HR-ToF-AMS (Lee et al., 2013;  
352 Farmer et al., 2010; Galloway et al., 2009). In this study, the typical normalized mass spectrum of N-  
353 containing fragments in SOA after 480 min of photo-oxidation reaction at different concentrations of  $\text{NH}_3$   
354 are given in Fig. 6. The prominent peaks in the  $\text{C}_x\text{H}_y\text{N}_n$  family were at  $m/z$  27 ( $\text{CHN}^+$ ), 30 ( $\text{CH}_4\text{N}^+$ ),  
355 40( $\text{C}_2\text{H}_2\text{N}^+$ ), 41( $\text{CHN}_2^+$ ,  $\text{C}_2\text{H}_3\text{N}^+$ ), 42( $\text{C}_2\text{H}_4\text{N}^+$ ), 43( $\text{C}_2\text{H}_5\text{N}^+$ ), 54( $\text{C}_2\text{H}_2\text{N}_2^+$ ,  $\text{C}_3\text{H}_4\text{N}^+$ ), 55( $\text{C}_3\text{H}_5\text{N}^+$ ), and  
356 68( $\text{C}_3\text{H}_4\text{N}_2^+$ ,  $\text{C}_4\text{H}_6\text{N}^+$ ); and the  $\text{C}_x\text{H}_y\text{O}_z\text{N}_n$  fragments were dominated by 45( $\text{CH}_3\text{ON}^+$ ), 46( $\text{CH}_4\text{ON}^+$ ),  
357 59( $\text{C}_2\text{H}_5\text{ON}^+$ ), 63( $\text{CH}_5\text{O}_2\text{N}^+$ ), 73( $\text{C}_2\text{H}_5\text{ON}_2^+$ ,  $\text{C}_3\text{H}_7\text{ON}^+$ ), 86( $\text{C}_3\text{H}_4\text{O}_2\text{N}^+$ ,  $\text{C}_3\text{H}_6\text{ON}_2^+$ ), 91( $\text{C}_3\text{H}_9\text{O}_2\text{N}^+$ ),  
358 97( $\text{C}_4\text{H}_5\text{ON}_2^+$ ), and 104( $\text{C}_3\text{H}_6\text{O}_3\text{N}^+$ ,  $\text{C}_4\text{H}_{10}\text{O}_2\text{N}^+$ ). The N-containing fragments observed in the experiment  
359 without added  $\text{NH}_3$  could be attributed to the reactions between organic peroxy ( $\text{RO}_2$ ) radicals and  $\text{NO}_x$   
360 (Arey et al., 2001) or uptake of background  $\text{NH}_3$  by SOA. Additionally, it was obvious that the signal  
361 intensities of most N-containing fragments became significantly stronger as the  $\text{NH}_3$  concentration increased  
362 (150–200 ppb). Therefore, a considerable amount of nitrogen-containing organics (the ratio of nitrogen-  
363 containing organics to SOA was about 6.7–7.7%) was formed during the photo-oxidation of gasoline vapor  
364 in the presence of  $\text{NH}_3$ . This was consistent with the previous study conducted by Liu et al. (2015c), who  
365 observed the formation of organic nitrogen compounds in the SOA generated from the OH oxidation of m-  
366 xylene. The promoting role of  $\text{NH}_3$  in the formation of N-containing species was also observed in the reaction  
367 system of ozonolysis and photo-oxidation of  $\alpha$ -pinene (Babar et al., 2017).

368 In addition, elemental analysis was also carried out to elucidate the SOA chemical composition and  
369 SOA formation mechanisms (Chhabra et al., 2011; Heald et al., 2010) at different concentrations of NH<sub>3</sub>.  
370 The time evolution of H/C and O/C in SOA formed from the photo-oxidation of gasoline vapor at different  
371 concentrations of NH<sub>3</sub> is shown in Fig. 7. As evident from Fig. 7, all data points are located in the triangular  
372 area for slope between -1 and 0, which suggests that SOA formation from the photo-oxidation of gasoline  
373 vapor is a combination of carboxylic acid and alcohol/peroxide (Heald et al., 2010). Moreover, in the  
374 presence of NH<sub>3</sub>, as shown in Fig. 8, N/C increased as reaction proceeded in the initial oxidation stage  
375 (0–120 min), accompanied by a rapid increase of O/C (0.12–0.67), a decrease of H/C (2.12–1.61), and a  
376 rapid formation of SOA. During this stage, the photo-oxidation of VOC precursors leads to a rapid increase  
377 in O/C and a rapid decrease in H/C. The termination chemistry of NO<sub>x</sub> with free radicals and the NH<sub>3</sub> uptake  
378 result in a rapid increase in N/C. As the reaction proceeded further (120–300 min), an increase of H/C which  
379 should be caused by NH<sub>3</sub> uptake resulted in an almost constant oxidation state of SOA in the continuous  
380 photo-oxidation, accompanied by an increase in the SOA concentration. Nozière et al. (2009) have reported  
381 that N-containing products would be generated from carbonyl compound (e.g., glyoxal) self-reactions  
382 catalyzed by NH<sub>4</sub><sup>+</sup> ions, which will have a dramatic impact on the volatility of oxidation products and the  
383 yield of SOA (Ortiz-Montalvo et al., 2014). In the last stage of the reaction (360–480 min), NH<sub>3</sub> uptake  
384 might reach saturation; therefore, H/C and N/C are almost constant. Comparing experiments with different  
385 concentrations of NH<sub>3</sub>, the average H/C shows an obvious increase (1.53–1.70) while the average O/C  
386 (0.70–0.78) shows a slight increase with the increase of NH<sub>3</sub> concentration (0–200 ppb), seen in Fig. S10.  
387 The slope in the Van Krevelen diagram shows a trend from slope = -1 to slope = 0 (Fig. S10), indicating that  
388 the formed carboxylic acid would further react with NH<sub>3</sub> via acid-base reaction to generate an ammonium  
389 salt of a carboxylate anion in the presence of NH<sub>3</sub> (Na et al., 2007). Xu et al. (2018) recently found that

390 imidazole products containing multiple oxygen atoms could be generated through heterogeneous reactions  
391 between NH<sub>3</sub> and carbonyl compounds (e.g., glyoxal), which might also contribute to the increase in the  
392 O/C of the SOA.

### 393 **3.4 Different roles of SO<sub>2</sub> and NH<sub>3</sub> in SOA chemical properties**

394 The chemical properties of the SOA generated under the different concentration of SO<sub>2</sub> or NH<sub>3</sub> were  
395 further compared by applying positive matrix factorization (PMF) analysis to the HR-ToF-AMS data,  
396 respectively (Chu et al., 2016; Liu et al., 2014). The details of PMF analysis are given in the Supplement.  
397 For the experiments under different SO<sub>2</sub> concentration conditions (i.e., Exps. GN, SGN1, SGN2, SGN3 and  
398 SGN4), two factors (Factor 1-S and Factor 2-S, Fig. S11a) were identified from the PMF analysis, and the  
399 difference mass spectra ( $m/z$  12–170) between the two factors and the time series of the mass concentrations  
400 are shown in Fig. 9. The intensity of C<sub>x</sub>H<sub>y</sub> and S-bearing organic fragments (C<sub>x</sub>H<sub>y</sub>O<sub>z</sub>S) in Factor 1-S was  
401 obviously stronger than that in Factor 2-S. Meanwhile, fragments in the high  $m/z$  range (> 110 Da) were  
402 more abundant in Factor 1-S (Fig. 9a, marked in red box). By contrast, the fragments containing oxygen in  
403 Factor 2-S were more abundant than in Factor 1-S, such as the typical fragment CO<sub>2</sub><sup>+</sup> ( $m/z$  44). Therefore,  
404 Factor 1-S was tentatively assigned to the less-oxygenated organic aerosol and oligomers, while Factor 2-S  
405 was more-oxygenated organic aerosol (Ulbrich et al., 2009). Similarly, for the experiments at different NH<sub>3</sub>  
406 concentration (i.e., Exps. GN, AGN1 and AGN2), two factors (Factor 1-N and Factor 2-N, Fig. S11b) were  
407 also identified in the same way. According to Fig. 10, Factor 1-N was tentatively assigned to the less-  
408 oxygenated organic aerosol and oligomers, while Factor 2-N was more-oxygenated organic aerosol and  
409 nitrogen-containing organics.

410 As shown in Fig. 9b and Fig. 10b, these two factors both had different time series during the entire  
411 reaction. With respect to Exps. GN, SGN1, SGN2, SGN3 and SGN4, Factor 1-S was formed later (~ 30 min)

412 than Factor 2-S, and then continuously increased during the entire reaction. Comparing experiments with  
413 different SO<sub>2</sub> concentrations, the maximum concentration of Factor 1-S, which was related to the less-  
414 oxygenated organic aerosol and oligomers, was enhanced with increased SO<sub>2</sub> concentration ( $R^2 = 0.881$ , Fig.  
415 9c). This suggested that the presence of SO<sub>2</sub> was prone to decrease the oxidation state of organic aerosol via  
416 acid-catalyzed reactions and enhance the formation of oligomers (Liu et al., 2016), which was consistent  
417 with the evolution of O/C vs. H/C shown in Fig. S12. Moreover, the gradually increasing concentration of  
418 Factor 1-S was related to the formation of sulfur-containing organics in the presence of SO<sub>2</sub> (Blair et al.,  
419 2017). By contrast, Factor 2-S was first gradually increased with the progress of the reaction and then  
420 decreased after reaching a peak (i.e., inflection point). And the time to reach the inflection point was affected  
421 by the SO<sub>2</sub> concentration (Fig. 9b). As the initial concentration of SO<sub>2</sub> increased from 0 ppb to 151 ppb, the  
422 time corresponding to the inflection point decreased, which indicated that the adverse influence of acid  
423 catalysis on Factor 2-S was gradually enhanced. In addition, the maximum concentration of Factor 2-S was  
424 negatively related with SO<sub>2</sub> concentration ( $R^2 = 0.987$ , Fig. 9c); this suggested that the presence of SO<sub>2</sub> and  
425 acid catalysis was adverse to the formation of more-oxygenated organic aerosol, leading to the decrease of  
426 the oxidation state of organic aerosol (Fig. S12).

427 By contrast, for Exps. GN, AGN1 and AGN2, Factor 1-N was first increased with the progress of the  
428 reaction and then gradually decreased after reaching a peak (Fig. 10b); while Factor 2-N was formed later  
429 (~ 30 min) than Factor 1-N, and then continuously increased during the entire reaction. This phenomenon  
430 was consistent with the expected behavior, that less-oxidized organic aerosol would be further oxidized to  
431 form more-oxidized organic aerosol. When comparing experiments with different NH<sub>3</sub> concentrations, it  
432 was observed that the concentration of Factor 2-N increased with increasing NH<sub>3</sub> concentration. Meanwhile,  
433 Factor 2-N, which was related to the more-oxidized organic aerosol and nitrogen-containing organics, was

434 a dominant factor in the presence of  $\text{NH}_3$ , and its maximum concentration was enhanced with the increase  
435 in  $\text{NH}_3$  concentration ( $R^2 = 0.988$ , Fig. 10c). Thence, the formation of more-oxygenated organic aerosol and  
436 nitrogen-containing organics will be enhanced with the increase of  $\text{NH}_3$  concentration. In contrast, a negative  
437 correlation was observed between the maximum concentration of Factor 1-N and  $\text{NH}_3$  concentration ( $R^2 =$   
438  $0.876$ , Fig. 10c); this revealed that less-oxygenated organic aerosol was gradually transformed to more  
439 oxidized species and nitrogen-containing organics in the presence of  $\text{NH}_3$ .

#### 440 **4 Conclusions**

441 In this study, SA formation from the photo-oxidation of gasoline/ $\text{NO}_x$  in the presence of  $\text{SO}_2$  or  $\text{NH}_3$   
442 was investigated. Our experimental results demonstrated that SA was enhanced by a factor of 1.6–2.6 or  
443 2.0–2.5, respectively, with the increase of  $\text{SO}_2$  or  $\text{NH}_3$  concentration (0–151 ppb and 0–200 ppb,  
444 respectively). Meanwhile, both secondary organic aerosol (SOA) and secondary inorganic aerosol (SIA)  
445 were increased by varying degrees. In the presence of  $\text{SO}_2$ ,  $\text{SO}_4^{2-}$  was the most sensitive linear increase with  
446 the increase of  $\text{SO}_2$  concentration, and SOA was also greatly enhanced due to the acid catalytic effect and  
447 the formation of sulfur-containing organics. In the presence of  $\text{NH}_3$ ,  $\text{NH}_4\text{NO}_3$  was most enhanced, following  
448 by SOA. The formation of nitrogen-containing organics was also promoted by the presence of  $\text{NH}_3$ .  
449 Meanwhile, conspicuous new particle formation (NPF) and particle size growth were enhanced in the  
450 presence of  $\text{SO}_2$  or  $\text{NH}_3$ .

451 In this study, a linear relationship between the SA yield and  $\text{SO}_2$  or  $\text{NH}_3$  concentration was also obtained  
452 (Fig. S13). Considering the typical concentrations of  $\text{SO}_2$  and  $\text{NH}_3$  of 40 ppb and 23 ppb in haze pollution  
453 in the north China plain (Cheng et al., 2016), and the lower aromatics content ( $\sim 10\%$ ) in vehicular  
454 evaporative emissions (Zhang et al., 2013), the SA yield is roughly estimated to be about 0.20. Recently, an  
455 updated emission inventory of vehicular evaporative emissions was reported to be  $1.65 \text{ Tg yr}^{-1}$  (Liu et al.,

2017a). Then, the SA formed from the photo-oxidation of VOCs emitted by vehicular evaporation in the presence of SO<sub>2</sub> and NH<sub>3</sub> is roughly estimated to be 0.33 Tg yr<sup>-1</sup>, which is about 1.5 times as much as the primary PM<sub>2.5</sub> emissions from transportation (0.21 Tg yr<sup>-1</sup>) in China (Jing et al., 2015; Zhang et al., 2007) and accounting for about 21 % of the SOA production (1.6 Tg yr<sup>-1</sup>) from anthropogenic precursors estimated by global chemical transport model (Farina et al., 2010). In addition, the photo-oxidation of long-chain alkanes (> C<sub>6</sub>, IVOCs) contained in evaporative emissions would also contribute to SOA formation (Pye and Pouliot, 2012; Tkacik et al., 2012; Presto et al., 2009; Lim and Ziemann, 2005; Zhao et al., 2016). This estimate suggests that vehicular evaporative emissions will be a significant source of SA in the presence of SO<sub>2</sub> and NH<sub>3</sub>, although the estimate might have a high uncertainty due to the fact that SA yield might vary considerably under different atmospheric conditions. Meanwhile, in the presence of NO<sub>x</sub>, SO<sub>2</sub> and NH<sub>3</sub>, vehicular evaporative emissions may be a potential source of sulfur- and nitrogen-containing organics, according to the results obtained from our study. Sulfur- and nitrogen-containing organics will have an adverse influence on the climate by light absorption and/or by affecting aerosol hygroscopicity (Staudt et al., 2014; Nguyen et al., 2012), and they also have a significant contribution to SOA and nitrogen or sulfur budgets (Lee et al., 2016; Shang et al., 2016).

Therefore, under the compound pollution conditions of SO<sub>2</sub> and NH<sub>3</sub>, synergistic emission reduction of vehicular evaporative emissions, SO<sub>2</sub> (e.g., coal-fired flue gas) and NH<sub>3</sub> (e.g., emitted from agricultural non-point source and traffic emissions) should be taken into consideration by policy makers for future management, which will contribute to reducing the burden of PM<sub>2.5</sub>, and then cut the environmental, economic and health costs caused by PM pollution. Our work will provide a scientific basis for taking corresponding control measures to relieve haze events in China. Additionally, there might be some differences between the VOCs composition of gasoline vapors directly injected to the smog chamber and

478 vehicular evaporative emissions. Thus, further work should be focused on SA formation directly from  
479 vehicular evaporative emissions under coexisting SO<sub>2</sub> and NH<sub>3</sub> conditions to shed light on the formation  
480 mechanism of SA under more atmospherically relevant conditions.

## 481 **Author contributions**

482 TZC and YCL contributed equally to this work and should be considered as co-first authors. HH, QXM,  
483 YCL, and TZC proposed the initial idea. YCL and TZC designed and led the study. YCL, BWC, QXM, PZ,  
484 and TZC conducted the data analyses. TZC, YCL, BWC, PZ, CGL, and JL interpreted the data. TZC, YCL,  
485 JL, and QXM wrote the manuscript, with inputs from all coauthors.

## 486 **Acknowledgements**

487 This work was financially supported by the National Key R&D Program of China (2016YFC0202700,  
488 2018YFC0506901), the National Natural Science Foundation of China (21876185, 41877306, 41877304,  
489 and 91744205), the special fund of the State Key Joint Laboratory of Environment Simulation and Pollution  
490 Control (17L01ESPC), the Youth Innovation Promotion Association, CAS (2018055, 2018060, and  
491 2017064), the Key Research Program of Frontier Sciences, CAS (QYZDB-SSW-DQC018), the National  
492 research program for key issues in air pollution control (DQGG0103), and the Young Talent Project of the  
493 Center for Excellence in Regional Atmospheric Environment, CAS (CERAE201801).

## 494 **References**

495 Arey, J., Aschmann, S. M., Kwok, E. S. C., and Atkinson, R.: Alkyl nitrate, hydroxyalkyl nitrate, and  
496 hydroxycarbonyl formation from the NO<sub>x</sub>-air photooxidations of C<sub>5</sub>-C<sub>8</sub> n-alkanes, *J. Phys. Chem. A*, 105, 1020-  
497 1027, doi: 10.1021/jp003292z, 2001.

498 Atkinson, R., and Arey, J.: Atmospheric degradation of volatile organic compounds, *Chem. Rev.*, 103, 4605-  
499 4638, doi: 10.1021/cr0206420, 2003.



500 Babar, Z. B., Park, J.-H., and Lim, H.-J.: Influence of NH<sub>3</sub> on secondary organic aerosols from the ozonolysis  
501 and photooxidation of  $\alpha$ -pinene in a flow reactor, *Atmos. Environ.*, 164, 71-84, doi:  
502 10.1016/j.atmosenv.2017.05.034, 2017.

503 Bahreini, R., Keywood, M. D., Ng, N. L., Varutbangkul, V., Gao, S., Flagan, R. C., Seinfeld, J. H., Worsnop,  
504 D. R., and Jimenez, J. L.: Measurements of secondary organic aerosol from oxidation of cycloalkenes, terpenes,  
505 and m-xylene using an Aerodyne aerosol mass spectrometer, *Environ. Sci. Technol.*, 39, 5674-5688, doi:  
506 10.1021/es048061a, 2005.

507 Bauduin, S., Clarisse, L., Hadji-Lazaro, J., Theys, N., Clerbaux, C., and Coheur, P. F.: Retrieval of near-  
508 surface sulfur dioxide (SO<sub>2</sub>) concentrations at a global scale using IASI satellite observations, *Atmo. Meas. Tech.*,  
509 9, 721-740, doi: 10.5194/amt-9-721-2016, 2016.

510 Blair, S. L., MacMillan, A. C., Drozd, G. T., Goldstein, A. H., Chu, R. K., Paša-Tolić, L., Shaw, J. B., Tolić,  
511 N., Lin, P., Laskin, J., Laskin, A., and Nizkorodov, S. A.: Molecular characterization of organosulfur compounds  
512 in biodiesel and diesel fuel secondary organic aerosol, *Environ. Sci. Technol.*, 51, 119-127, doi:  
513 10.1021/acs.est.6b03304, 2017.

514 Calvert, J. G., Atkinson, R., Becker, K. H., Kamens, R. M., Seinfeld, J. H., Wallington, T. H., and Yarwood,  
515 G.: *The mechanisms of atmospheric oxidation of the aromatic hydrocarbons*, Oxford University Press, 2002.

516 Cao, G., and Jang, M.: Effects of particle acidity and UV light on secondary organic aerosol formation from  
517 oxidation of aromatics in the absence of NO<sub>x</sub>, *Atmos. Environ.*, 41, 7603-7613, doi:  
518 10.1016/j.atmosenv.2007.05.034, 2007.

519 Casale, M. T., Richman, A. R., Elrod, M. J., Garland, R. M., Beaver, M. R., and Tolbert, M. A.: Kinetics of  
520 acid-catalyzed aldol condensation reactions of aliphatic aldehydes, *Atmos. Environ.*, 41, 6212-6224, doi:  
521 10.1016/j.atmosenv.2007.04.002, 2007.

522 Chapleski, R. C., Zhang, Y., Troya, D., and Morris, J. R.: Heterogeneous chemistry and reaction dynamics  
523 of the atmospheric oxidants, O<sub>3</sub>, NO<sub>3</sub>, and OH, on organic surfaces, *Chem. Soc. Rev.*, 45, 3731-3746, doi:  
524 10.1039/C5CS00375J, 2016.

525 Chen, T., Liu, Y., Chu, B., Liu, C., Liu, J., Ge, Y., Ma, Q., Ma, J., and He, H.: Differences of the oxidation  
526 process and secondary organic aerosol formation at low and high precursor concentrations, *J. Environ. Sci.*, 79,  
527 256-263, doi: 10.1016/j.jes.2018.11.011, 2019a.

528 Chen, T., Liu, Y., Liu, C., Liu, J., Chu, B., and He, H.: Important role of aromatic hydrocarbons in SOA  
529 formation from unburned gasoline vapor, *Atmos. Environ.*, 201, 101-109, doi: 10.1016/j.atmosenv.2019.01.001,  
530 2019b.

531 Cheng, Y., Li, S.-M., and Leithead, A.: Chemical characteristics and origins of nitrogen-containing organic  
532 compounds in PM<sub>2.5</sub> aerosols in the Lower Fraser Valley, *Environ. Sci. Technol.*, 40, 5846-5852, doi:  
533 10.1021/es0603857, 2006.

534 Cheng, Y., Zheng, G., Wei, C., Mu, Q., Zheng, B., Wang, Z., Gao, M., Zhang, Q., He, K., Carmichael, G.,  
535 Pöschl, U., and Su, H.: Reactive nitrogen chemistry in aerosol water as a source of sulfate during haze events in  
536 China, *Sci. Adv.*, 2, doi: 10.1126/sciadv.1601530, 2016.

537 Chhabra, P. S., Ng, N. L., Canagaratna, M. R., Corrigan, A. L., Russell, L. M., Worsnop, D. R., Flagan, R.  
538 C., and Seinfeld, J. H.: Elemental composition and oxidation of chamber organic aerosol, *Atmos. Chem. Phys.*,  
539 11, 8827-8845, doi: 10.5194/acp-11-8827-2011, 2011.

540 Chu, B., Kerminen, V. M., Bianchi, F., Yan, C., Petäjä, T., and Kulmala, M.: Atmospheric new particle  
541 formation in China, *Atmos. Chem. Phys.*, 19, 115-138, doi: 10.5194/acp-19-115-2019, 2019.

542 Chu, B., Zhang, X., Liu, Y., He, H., Sun, Y., Jiang, J., Li, J., and Hao, J.: Synergetic formation of secondary  
543 inorganic and organic aerosol: effect of SO<sub>2</sub> and NH<sub>3</sub> on particle formation and growth, *Atmos. Chem. Phys.*, 16,

544 14219-14230, doi: 10.5194/acp-16-14219-2016, 2016.

545 Clegg, S. L., Brimblecombe, P., and Wexler, A. S.: Thermodynamic model of the system  $\text{H}^+ - \text{NH}_4^+ - \text{SO}_4^{2-}$   
546  $- \text{NO}_3^- - \text{H}_2\text{O}$  at tropospheric temperatures, *J. Phys. Chem. A*, 102, 2137-2154, doi: 10.1021/jp973042r, 1998.

547 Clegg, S. L., and Brimblecombe, P.: Comment on the “Thermodynamic Dissociation Constant of the  
548 Bisulfate Ion from Raman and Ion Interaction Modeling Studies of Aqueous Sulfuric Acid at Low Temperatures”,  
549 *J. Phys. Chem. A*, 109, 2703-2706, doi: 10.1021/jp0401170, 2005.

550 Czoschke, N. M., Jang, M., and Kamens, R. M.: Effect of acidic seed on biogenic secondary organic aerosol  
551 growth, *Atmos. Environ.*, 37, 4287-4299, doi: 10.1016/S1352-2310(03)00511-9, 2003.

552 Davidson, C. I., Phalen, R. F., and Solomon, P. A.: Airborne particulate matter and human health: a review,  
553 *Aerosol Sci. Tech.*, 39, 737-749, doi: 10.1080/02786820500191348, 2005.

554 DeCarlo, P. F., Slowik, J. G., Worsnop, D. R., Davidovits, P., and Jimenez, J. L.: Particle morphology and  
555 density characterization by combined mobility and aerodynamic diameter measurements. Part 1: Theory, *Aerosol*  
556 *Sci. Tech.*, 38, 1185-1205, doi: 10.1080/027868290903907, 2004.

557 Díaz-de-Mera, Y., Aranda, A., Martínez, E., Rodríguez, A. A., Rodríguez, D., and Rodríguez, A.: Formation  
558 of secondary aerosols from the ozonolysis of styrene: effect of  $\text{SO}_2$  and  $\text{H}_2\text{O}$ , *Atmos. Environ.*, 171, 25-31, doi:  
559 10.1016/j.atmosenv.2017.10.011, 2017.

560 Donahue, N. M., Robinson, A. L., Stanier, C. O., and Pandis, S. N.: Coupled partitioning, dilution, and  
561 chemical aging of semivolatile organics, *Environ. Sci. Technol.*, 40, 2635-2643, doi: 10.1021/es052297c, 2006.

562 Drewnick, F., Hings, S. S., DeCarlo, P., Jayne, J. T., Gonin, M., Fuhrer, K., Weimer, S., Jimenez, J. L.,  
563 Demerjian, K. L., Borrmann, S., and Worsnop, D. R.: A new time-of-flight aerosol mass spectrometer (TOF-  
564 AMS)—instrument description and first field deployment, *Aerosol Sci. Tech.*, 39, 637-658, doi:  
565 10.1080/02786820500182040, 2005.

566 Edney, E. O., Kleindienst, T. E., Jaoui, M., Lewandowski, M., Offenberg, J. H., Wang, W., and Claeys, M.:  
567 Formation of 2-methyl tetrols and 2-methylglyceric acid in secondary organic aerosol from laboratory irradiated  
568 isoprene/NO<sub>x</sub>/SO<sub>2</sub>/air mixtures and their detection in ambient PM<sub>2.5</sub> samples collected in the eastern United States,  
569 *Atmos. Environ.*, 39, 5281-5289, doi: 10.1016/j.atmosenv.2005.05.031, 2005.

570 Farmer, D. K., Matsunaga, A., Docherty, K. S., Surratt, J. D., Seinfeld, J. H., Ziemann, P. J., and Jimenez, J.  
571 L.: Response of an aerosol mass spectrometer to organonitrates and organosulfates and implications for  
572 atmospheric chemistry, *Proc. Natl. Acad. Sci. USA*, 107, 6670-6675, doi: 10.1073/pnas.0912340107, 2010.

573 Fu, X., Wang, S. X., Ran, L. M., Pleim, J. E., Cooter, E., Bash, J. O., Benson, V., and Hao, J. M.: Estimating  
574 NH<sub>3</sub> emissions from agricultural fertilizer application in China using the bi-directional CMAQ model coupled to  
575 an agro-ecosystem model, *Atmos. Chem. Phys.*, 15, 6637-6649, doi: 10.5194/acp-15-6637-2015, 2015.

576 Galloway, M. M., Chhabra, P. S., Chan, A. W. H., Surratt, J. D., Flagan, R. C., Seinfeld, J. H., and Keutsch,  
577 F. N.: Glyoxal uptake on ammonium sulphate seed aerosol: reaction products and reversibility of uptake under  
578 dark and irradiated conditions, *Atmos. Chem. Phys.*, 9, 3331-3345, doi: 10.5194/acp-9-3331-2009, 2009.

579 Gordon, T. D., Presto, A. A., May, A. A., Nguyen, N. T., Lipsky, E. M., Donahue, N. M., Gutierrez, A.,  
580 Zhang, M., Maddox, C., Rieger, P., Chattopadhyay, S., Maldonado, H., Maricq, M. M., and Robinson, A. L.:  
581 Secondary organic aerosol formation exceeds primary particulate matter emissions for light-duty gasoline vehicles,  
582 *Atmos. Chem. Phys.*, 14, 4661-4678, doi: 10.5194/acp-14-4661-2014, 2014.

583 Guo, S., Hu, M., Zamora, M. L., Peng, J., Shang, D., Zheng, J., Du, Z., Wu, Z., Shao, M., Zeng, L., Molina,  
584 M. J., and Zhang, R.: Elucidating severe urban haze formation in China, *Proc. Natl. Acad. Sci. USA*, 111, 17373-  
585 17378, doi: 10.1073/pnas.1419604111, 2014.

586 Hallquist, M., Wenger, J. C., Baltensperger, U., Rudich, Y., Simpson, D., Claeys, M., Dommen, J., Donahue,  
587 N. M., George, C., Goldstein, A. H., Hamilton, J. F., Herrmann, H., Hoffmann, T., Iinuma, Y., Jang, M., Jenkin,

588 M. E., Jimenez, J. L., Kiendler-Scharr, A., Maenhaut, W., McFiggans, G., Mentel, T. F., Monod, A., Prévôt, A. S.  
589 H., Seinfeld, J. H., Surratt, J. D., Szmigielski, R., and Wildt, J.: The formation, properties and impact of secondary  
590 organic aerosol: current and emerging issues, *Atmos. Chem. Phys.*, 9, 5155-5236, doi: 10.5194/acp-9-5155-2009,  
591 2009.

592 Hatch, L. E., Creamean, J. M., Ault, A. P., Surratt, J. D., Chan, M. N., Seinfeld, J. H., Edgerton, E. S., Su, Y.,  
593 and Prather, K. A.: Measurements of isoprene-derived organosulfates in ambient aerosols by aerosol time-of-flight  
594 mass spectrometry—Part 2: temporal variability and formation mechanisms, *Environ. Sci. Technol.*, 45, 8648-  
595 8655, doi: 10.1021/es2011836, 2011.

596 He, H., Wang, Y., Ma, Q., Ma, J., Chu, B., Ji, D., Tang, G., Liu, C., Zhang, H., and Hao, J.: Mineral dust and  
597 NO<sub>x</sub> promote the conversion of SO<sub>2</sub> to sulfate in heavy pollution days, *Sci. Rep.*, 4, 4172, doi: 10.1038/srep04172,  
598 2014.

599 Heald, C. L., Kroll, J. H., Jimenez, J. L., Docherty, K. S., DeCarlo, P. F., Aiken, A. C., Chen, Q., Martin, S.  
600 T., Farmer, D. K., and Artaxo, P.: A simplified description of the evolution of organic aerosol composition in the  
601 atmosphere, *Geophys. Res. Lett.*, 37, L08803, doi: 10.1029/2010GL042737, 2010.

602 Hou, S., Tong, S., Ge, M., and An, J.: Comparison of atmospheric nitrous acid during severe haze and clean  
603 periods in Beijing, China, *Atmos. Environ.*, 124, 199-206, doi: 10.1016/j.atmosenv.2015.06.023, 2016.

604 Huang, D. D., Li, Y. J., Lee, B. P., and Chan, C. K.: Analysis of organic sulfur compounds in atmospheric  
605 aerosols at the HKUST supersite in Hong Kong using HR-ToF-AMS, *Environ. Sci. Technol.*, 49, 3672-3679, doi:  
606 10.1021/es5056269, 2015.

607 Huang, R.-J., Zhang, Y., Bozzetti, C., Ho, K.-F., Cao, J.-J., Han, Y., Daellenbach, K. R., Slowik, J. G., Platt,  
608 S. M., Canonaco, F., Zotter, P., Wolf, R., Pieber, S. M., Bruns, E. A., Crippa, M., Ciarelli, G., Piazzalunga, A.,  
609 Schwikowski, M., Abbaszade, G., Schnelle-Kreis, J., Zimmermann, R., An, Z., Szidat, S., Baltensperger, U.,

610 Haddad, I. E., and Prevot, A. S. H.: High secondary aerosol contribution to particulate pollution during haze events  
611 in China, *Nature*, 514, 218-222, doi: 10.1038/nature13774, 2014.

612 Ianniello, A., Spataro, F., Esposito, G., Allegrini, I., Rantica, E., Ancora, M. P., Hu, M., and Zhu, T.:  
613 Occurrence of gas phase ammonia in the area of Beijing (China), *Atmos. Chem. Phys.*, 10, 9487-9503, doi:  
614 10.5194/acp-10-9487-2010, 2010.

615 Jang, M., and Kamens, R. M.: Atmospheric secondary aerosol formation by heterogeneous reactions of  
616 aldehydes in the presence of a sulfuric acid aerosol catalyst, *Environ. Sci. Technol.*, 35, 4758-4766, doi:  
617 10.1021/es010790s, 2001.

618 Jang, M., Czoschke, N. M., Lee, S., and Kamens, R. M.: Heterogeneous atmospheric aerosol production by  
619 acid-catalyzed particle-phase reactions, *Science*, 298, 814-817, doi: 10.1126/science.1075798, 2002.

620 Jang, M., Carroll, B., Chandramouli, B., and Kamens, R. M.: Particle growth by acid-catalyzed  
621 heterogeneous reactions of organic carbonyls on preexisting aerosols, *Environ. Sci. Technol.*, 37, 3828-3837, doi:  
622 10.1021/es021005u, 2003a.

623 Jang, M., Lee, S., and Kamens, R. M.: Organic aerosol growth by acid-catalyzed heterogeneous reactions of  
624 octanal in a flow reactor, *Atmos. Environ.*, 37, 2125-2138, doi: 10.1016/S1352-2310(03)00077-3, 2003b.

625 Jaoui, M., Edney, E. O., Kleindienst, T. E., Lewandowski, M., Offenberg, J. H., Surratt, J. D., and Seinfeld,  
626 J. H.: Formation of secondary organic aerosol from irradiated  $\alpha$ -pinene/toluene/NO<sub>x</sub> mixtures and the effect of  
627 isoprene and sulfur dioxide, *J. Geophys. Res.-Atmos.*, 113, doi: 10.1029/2007jd009426, 2008.

628 Jathar, S. H., Gordon, T. D., Hennigan, C. J., Pye, H. O. T., Pouliot, G., Adams, P. J., Donahue, N. M., and  
629 Robinson, A. L.: Unspeciated organic emissions from combustion sources and their influence on the secondary  
630 organic aerosol budget in the United States, *Proc. Natl. Acad. Sci. USA*, 111, 10473-10478, doi:  
631 10.1073/pnas.1323740111, 2014.

632 Jayne, J. T., Leard, D. C., Zhang, X., Davidovits, P., Smith, K. A., Kolb, C. E., and Worsnop, D. R.:  
633 Development of an aerosol mass spectrometer for size and composition analysis of submicron particles, *Aerosol*  
634 *Sci. Tech.*, 33, 49-70, doi: 10.1080/027868200410840, 2000.

635 Jiang, B., and Xia, D.: Role identification of NH<sub>3</sub> in atmospheric secondary new particle formation in haze  
636 occurrence of China, *Atmos. Environ.*, 163, 107-117, doi: 10.1016/j.atmosenv.2017.05.035, 2017.

637 Jimenez, J. L., Canagaratna, M. R., Donahue, N. M., Prevot, A. S. H., Zhang, Q., Kroll, J. H., DeCarlo, P. F.,  
638 Allan, J. D., Coe, H., Ng, N. L., Aiken, A. C., Docherty, K. S., Ulbrich, I. M., Grieshop, A. P., Robinson, A. L.,  
639 Duplissy, J., Smith, J. D., Wilson, K. R., Lanz, V. A., Hueglin, C., Sun, Y. L., Tian, J., Laaksonen, A., Raatikainen,  
640 T., Rautiainen, J., Vaattovaara, P., Ehn, M., Kulmala, M., Tomlinson, J. M., Collins, D. R., Cubison, M. J., Dunlea,  
641 J., Huffman, J. A., Onasch, T. B., Alfarra, M. R., Williams, P. I., Bower, K., Kondo, Y., Schneider, J., Drewnick,  
642 F., Borrmann, S., Weimer, S., Demerjian, K., Salcedo, D., Cottrell, L., Griffin, R., Takami, A., Miyoshi, T.,  
643 Hatakeyama, S., Shimojo, A., Sun, J. Y., Zhang, Y. M., Dzepina, K., Kimmel, J. R., Sueper, D., Jayne, J. T.,  
644 Herndon, S. C., Trimborn, A. M., Williams, L. R., Wood, E. C., Middlebrook, A. M., Kolb, C. E., Baltensperger,  
645 U., and Worsnop, D. R.: Evolution of organic aerosols in the atmosphere, *Science*, 326, 1525-1529, doi:  
646 10.1126/science.1180353, 2009.

647 Jimenez, J. L., Jayne, J. T., Shi, Q., Kolb, C. E., Worsnop, D. R., Yourshaw, I., Seinfeld, J. H., Flagan, R. C.,  
648 Zhang, X., Smith, K. A., Morris, J. W., and Davidovits, P.: Ambient aerosol sampling using the aerodyne aerosol  
649 mass spectrometer, *J Geophys Res Atmos*, 108, doi: 10.1029/2001JD001213, 2003.

650 Jing, M., Junfeng, L., Yuan, X., and Shu, T.: Tracing primary PM<sub>2.5</sub> emissions via Chinese supply chains,  
651 *Environ. Res. Lett.*, 10, 054005, 2015.

652 Kang, Y., Liu, M., Song, Y., Huang, X., Yao, H., Cai, X., Zhang, H., Kang, L., Liu, X., Yan, X., He, H.,  
653 Zhang, Q., Shao, M., and Zhu, T.: High-resolution ammonia emissions inventories in China from 1980 to 2012,

654 Atmos. Chem. Phys., 16, 2043-2058, doi: 10.5194/acp-16-2043-2016, 2016.

655 Kleindienst, T. E., Edney, E. O., Lewandowski, M., Offenberg, J. H., and Jaoui, M.: Secondary organic  
656 carbon and aerosol yields from the irradiations of isoprene and  $\alpha$ -pinene in the presence of NO<sub>x</sub> and SO<sub>2</sub>, Environ.  
657 Sci. Technol., 40, 3807-3812, doi: 10.1021/es052446r, 2006.

658 Krechmer, J. E., Pagonis, D., Ziemann, P. J., and Jimenez, J. L.: Quantification of gas-wall partitioning in  
659 Teflon environmental chambers using rapid bursts of low-volatility oxidized species generated in situ, Environ.  
660 Sci. Technol., 50, 5757-5765, doi: 10.1021/acs.est.6b00606, 2016.

661 Kroll, J. H., Donahue, N. M., Jimenez, J. L., Kessler, S. H., Canagaratna, M. R., Wilson, K. R., Altieri, K.  
662 E., Mazzoleni, L. R., Wozniak, A. S., Bluhm, H., Mysak, E. R., Smith, J. D., Kolb, C. E., and Worsnop, D. R.:  
663 Carbon oxidation state as a metric for describing the chemistry of atmospheric organic aerosol, Nat. Chem., 3,  
664 133, doi: 10.1038/nchem.948, 2011.

665 Kroll, J. H., and Seinfeld, J. H.: Chemistry of secondary organic aerosol: Formation and evolution of low-  
666 volatility organics in the atmosphere, Atmos. Environ., 42, 3593-3624, doi: 10.1016/j.atmosenv.2008.01.003,  
667 2008.

668 Kundu, S., Quraishi, T. A., Yu, G., Suarez, C., Keutsch, F. N., and Stone, E. A.: Evidence and quantitation  
669 of aromatic organosulfates in ambient aerosols in Lahore, Pakistan, Atmos. Chem. Phys., 13, 4865-4875, doi:  
670 10.5194/acp-13-4865-2013, 2013.

671 Lee, A. K. Y., Zhao, R., Li, R., Liggio, J., Li, S.-M., and Abbatt, J. P. D.: Formation of light absorbing organo-  
672 nitrogen species from evaporation of droplets containing glyoxal and ammonium sulfate, Environ. Sci. Technol.,  
673 47, 12819-12826, doi: 10.1021/es402687w, 2013.

674 Lee, B. H., Mohr, C., Lopez-Hilfiker, F. D., Lutz, A., Hallquist, M., Lee, L., Romer, P., Cohen, R. C., Iyer,  
675 S., Kurtén, T., Hu, W., Day, D. A., Campuzano-Jost, P., Jimenez, J. L., Xu, L., Ng, N. L., Guo, H., Weber, R. J.,



676 Wild, R. J., Brown, S. S., Koss, A., de Gouw, J., Olson, K., Goldstein, A. H., Seco, R., Kim, S., McAvey, K.,  
677 Shepson, P. B., Starn, T., Baumann, K., Edgerton, E. S., Liu, J., Shilling, J. E., Miller, D. O., Brune, W.,  
678 Schobesberger, S., D'Ambro, E. L., and Thornton, J. A.: Highly functionalized organic nitrates in the southeast  
679 United States: Contribution to secondary organic aerosol and reactive nitrogen budgets, *Proc. Natl. Acad. Sci.*  
680 *USA*, 113, 1516-1521, doi: 10.1073/pnas.1508108113, 2016.

681 Li, K., Chen, L., White, S. J., Yu, H., Wu, X., Gao, X., Azzi, M., and Cen, K.: Smog chamber study of the  
682 role of NH<sub>3</sub> in new particle formation from photo-oxidation of aromatic hydrocarbons, *Sci. Total Environ.*, 619-  
683 620, 927-937, doi: 10.1016/j.scitotenv.2017.11.180, 2018.

684 Li, L., Tan, Q., Zhang, Y., Feng, M., Qu, Y., An, J., and Liu, X.: Characteristics and source apportionment of  
685 PM<sub>2.5</sub> during persistent extreme haze events in Chengdu, southwest China, *Environ. Pollut.*, 230, 718-729, doi:  
686 10.1016/j.envpol.2017.07.029, 2017.

687 Liggio, J., Li, S.-M., and McLaren, R.: Heterogeneous reactions of glyoxal on particulate matter:  
688 identification of acetals and sulfate esters, *Environ. Sci. Technol.*, 39, 1532-1541, doi: 10.1021/es048375y, 2005.

689 Liggio, J., and Li, S. M.: Reactive uptake of pinonaldehyde on acidic aerosols, *J. Geophys. Res.-Atmos.*, 111,  
690 doi: doi:10.1029/2005JD006978, 2006.

691 Liggio, J., Li, S. M., Brook, J. R., and Mihele, C.: Direct polymerization of isoprene and  $\alpha$ -pinene on acidic  
692 aerosols, *Geophys. Res. Lett.*, 34, doi: 10.1029/2006GL028468, 2007.

693 Liggio, J., and Li, S. M.: Reversible and irreversible processing of biogenic olefins on acidic aerosols, *Atmos.*  
694 *Chem. Phys.*, 8, 2039-2055, doi: 10.5194/acp-8-2039-2008, 2008.

695 Lim, Y. B., and Ziemann, P. J.: Products and mechanism of secondary organic aerosol formation from  
696 reactions of n-alkanes with OH radicals in the presence of NO<sub>x</sub>, *Environ. Sci. Technol.*, 39, 9229-9236, doi:  
697 10.1021/es051447g, 2005.

698 Lin, Y. H., Knipping, E. M., Edgerton, E. S., Shaw, S. L., and Surratt, J. D.: Investigating the influences of  
699 SO<sub>2</sub> and NH<sub>3</sub> levels on isoprene-derived secondary organic aerosol formation using conditional sampling  
700 approaches, *Atmos. Chem. Phys.*, 13, 8457-8470, doi: 10.5194/acp-13-8457-2013, 2013.

701 Liu, H., Man, H., Cui, H., Wang, Y., Deng, F., Wang, Y., Yang, X., Xiao, Q., Zhang, Q., Ding, Y., and He, K.:  
702 An updated emission inventory of vehicular VOCs and IVOCs in China, *Atmos. Chem. Phys.*, 17, 12709-12724,  
703 doi: 10.5194/acp-17-12709-2017, 2017a.

704 Liu, S., Jia, L., Xu, Y., Tsona, N. T., Ge, S., and Du, L.: Photooxidation of cyclohexene in the presence of  
705 SO<sub>2</sub>: SOA yield and chemical composition, *Atmos. Chem. Phys.*, 17, 13329-13343, doi: 10.5194/acp-17-13329-  
706 2017, 2017b.

707 Liu, T., Wang, X., Deng, W., Hu, Q., Ding, X., Zhang, Y., He, Q., Zhang, Z., Lü, S., Bi, X., Chen, J., and Yu,  
708 J.: Secondary organic aerosol formation from photochemical aging of light-duty gasoline vehicle exhausts in a  
709 smog chamber, *Atmos. Chem. Phys.*, 15, 9049-9062, doi: 10.5194/acp-15-9049-2015, 2015a.

710 Liu, T., Wang, X., Deng, W., Zhang, Y., Chu, B., Ding, X., Hu, Q., He, H., and Hao, J.: Role of ammonia in  
711 forming secondary aerosols from gasoline vehicle exhaust, *Sci. China Chem.*, 58, 1377-1384, doi:  
712 10.1007/s11426-015-5414-x, 2015b.

713 Liu, T., Wang, X., Hu, Q., Deng, W., Zhang, Y., Ding, X., Fu, X., Bernard, F., Zhang, Z., Lü, S., He, Q., Bi,  
714 X., Chen, J., Sun, Y., Yu, J., Peng, P., Sheng, G., and Fu, J.: Formation of secondary aerosols from gasoline vehicle  
715 exhaust when mixing with SO<sub>2</sub>, *Atmos. Chem. Phys.*, 16, 675-689, doi: 10.5194/acp-16-675-2016, 2016.

716 Liu, X. G., Li, J., Qu, Y., Han, T., Hou, L., Gu, J., Chen, C., Yang, Y., Liu, X., Yang, T., Zhang, Y., Tian, H.,  
717 and Hu, M.: Formation and evolution mechanism of regional haze: a case study in the megacity Beijing, China,  
718 *Atmos. Chem. Phys.*, 13, 4501-4514, doi: 10.5194/acp-13-4501-2013, 2013.

719 Liu, Y., Li, S. M., and Liggió, J.: Technical Note: application of positive matrix factor analysis in

720 heterogeneous kinetics studies utilizing the mixed-phase relative rates technique, *Atmos. Chem. Phys.*, 14, 9201-  
721 9211, doi: 10.5194/acp-14-9201-2014, 2014.

722 Liu, Y., Liggió, J., Staebler, R., and Li, S. M.: Reactive uptake of ammonia to secondary organic aerosols:  
723 kinetics of organonitrogen formation, *Atmos. Chem. Phys.*, 15, 13569-13584, doi: 10.5194/acp-15-13569-2015,  
724 2015c.

725 Liu, Y., Shao, M., Fu, L., Lu, S., Zeng, L., and Tang, D.: Source profiles of volatile organic compounds  
726 (VOCs) measured in China: Part I, *Atmos. Environ.*, 42, 6247-6260, doi: 10.1016/j.atmosenv.2008.01.070, 2008.

727 Lu, Z., Streets, D. G., Zhang, Q., Wang, S., Carmichael, G. R., Cheng, Y. F., Wei, C., Chin, M., Diehl, T.,  
728 and Tan, Q.: Sulfur dioxide emissions in China and sulfur trends in East Asia since 2000, *Atmos. Chem. Phys.*,  
729 10, 6311-6331, doi: 10.5194/acp-10-6311-2010, 2010.

730 Meade, L. E., Riva, M., Blomberg, M. Z., Brock, A. K., Qualters, E. M., Siejack, R. A., Ramakrishnan, K.,  
731 Surratt, J. D., and Kautzman, K. E.: Seasonal variations of fine particulate organosulfates derived from biogenic  
732 and anthropogenic hydrocarbons in the mid-Atlantic United States, *Atmos. Environ.*, 145, 405-414, doi:  
733 10.1016/j.atmosenv.2016.09.028, 2016.

734 Meng, Z. Y., Lin, W. L., Jiang, X. M., Yan, P., Wang, Y., Zhang, Y. M., Jia, X. F., and Yu, X. L.:  
735 Characteristics of atmospheric ammonia over Beijing, China, *Atmos. Chem. Phys.*, 11, 6139-6151, doi:  
736 10.5194/acp-11-6139-2011, 2011.

737 Na, K., Song, C., and Cocker, D. R.: Formation of secondary organic aerosol from the reaction of styrene  
738 with ozone in the presence and absence of ammonia and water, *Atmos. Environ.*, 40, 1889-1900, doi:  
739 10.1016/j.atmosenv.2005.10.063, 2006.

740 Na, K., Song, C., Switzer, C., and Cocker, D. R.: Effect of ammonia on secondary organic aerosol formation  
741 from  $\alpha$ -pinene ozonolysis in dry and humid conditions, *Environ. Sci. Technol.*, 41, 6096-6102, doi:

742 10.1021/es061956y, 2007.

743 Nguyen, T. B., Lee, P. B., Updyke, K. M., Bones, D. L., Laskin, J., Laskin, A., and Nizkorodov, S. A.:

744 Formation of nitrogen- and sulfur-containing light-absorbing compounds accelerated by evaporation of water

745 from secondary organic aerosols, *J. Geophys. Res.-Atmos.*, 117, doi: 10.1029/2011jd016944, 2012.

746 Nozière, B., Dziedzic, P., and Córdova, A.: Products and kinetics of the liquid-phase reaction of glyoxal

747 catalyzed by ammonium ions ( $\text{NH}_4^+$ ), *J. Phys. Chem. A*, 113, 231-237, doi: 10.1021/jp8078293, 2009.

748 Ortiz-Montalvo, D. L., Häkkinen, S. A. K., Schwier, A. N., Lim, Y. B., McNeill, V. F., and Turpin, B. J.:

749 Ammonium addition (and aerosol pH) has a dramatic impact on the volatility and yield of glyoxal secondary

750 organic aerosol, *Environ. Sci. Technol.*, 48, 255-262, doi: 10.1021/es4035667, 2014.

751 Pan, Y., Tian, S., Liu, D., Fang, Y., Zhu, X., Zhang, Q., Zheng, B., Michalski, G., and Wang, Y.: Fossil fuel

752 combustion-related emissions dominate atmospheric ammonia sources during severe haze episodes: Evidence

753 from  $^{15}\text{N}$ -stable isotope in size-resolved aerosol ammonium, *Environ. Sci. Technol.*, 50, 8049-8056, doi:

754 10.1021/acs.est.6b00634, 2016.

755 Platt, S. M., El Haddad, I., Zardini, A. A., Clairotte, M., Astorga, C., Wolf, R., Slowik, J. G., Temime-Roussel,

756 B., Marchand, N., Ježek, I., Drinovec, L., Močnik, G., Möhler, O., Richter, R., Barmet, P., Bianchi, F.,

757 Baltensperger, U., and Prévôt, A. S. H.: Secondary organic aerosol formation from gasoline vehicle emissions in

758 a new mobile environmental reaction chamber, *Atmos. Chem. Phys.*, 13, 9141-9158, doi: 10.5194/acp-13-9141-

759 2013, 2013.

760 Pöschl, U.: Atmospheric aerosols: composition, transformation, climate and health effects, *Angew. Chem.*

761 *Int. Ed.*, 44, 7520-7540, doi: 10.1002/anie.200501122, 2005.

762 Presto, A. A., Miracolo, M. A., Kroll, J. H., Worsnop, D. R., Robinson, A. L., and Donahue, N. M.:

763 Intermediate-volatility organic compounds: A potential source of ambient oxidized organic aerosol, *Environ. Sci.*

764 Technol., 43, 4744-4749, doi: 10.1021/es803219q, 2009.

765 Pye, H. O. T., and Pouliot, G. A.: Modeling the role of alkanes, polycyclic aromatic hydrocarbons, and their  
766 oligomers in secondary organic aerosol formation, Environ. Sci. Technol., 46, 6041-6047, doi:  
767 10.1021/es300409w, 2012.

768 Riva, M., Tomaz, S., Cui, T., Lin, Y.-H., Perraudin, E., Gold, A., Stone, E. A., Villenave, E., and Surratt, J.  
769 D.: Evidence for an unrecognized secondary anthropogenic source of organosulfates and sulfonates: gas-phase  
770 oxidation of polycyclic aromatic hydrocarbons in the presence of sulfate aerosol, Environ. Sci. Technol., 49, 6654-  
771 6664, doi: 10.1021/acs.est.5b00836, 2015.

772 Riva, M., Da Silva Barbosa, T., Lin, Y. H., Stone, E. A., Gold, A., and Surratt, J. D.: Chemical  
773 characterization of organosulfates in secondary organic aerosol derived from the photooxidation of alkanes,  
774 Atmos. Chem. Phys., 16, 11001-11018, doi: 10.5194/acp-16-11001-2016, 2016.

775 Rollins, A. W., Kiendler-Scharr, A., Fry, J. L., Brauers, T., Brown, S. S., Dorn, H. P., Dube, W. P., Fuchs, H.,  
776 Mensah, A., Mentel, T. F., Rohrer, F., Tillmann, R., Wegener, R., Wooldridge, P. J., and Cohen, R. C.: Isoprene  
777 oxidation by nitrate radical: Alkyl nitrate and secondary organic aerosol yields, Atmos. Chem. Phys., 9, 6685-  
778 6703, doi: 10.5194/acp-9-6685-2009, 2009.

779 Santiago, M., Garcia Vivanco, M., and Stein, A. F.: SO<sub>2</sub> effect on secondary organic aerosol from a mixture  
780 of anthropogenic VOCs: experimental and modelled results, Int. J. Environ. Pollut., 50, 224-233, doi:  
781 10.1504/ijep.2012.051195, 2012.

782 Sato, K., Takami, A., Isozaki, T., Hikida, T., Shimono, A., and Imamura, T.: Mass spectrometric study of  
783 secondary organic aerosol formed from the photo-oxidation of aromatic hydrocarbons, Atmos. Environ., 44, 1080-  
784 1087, doi: 10.1016/j.atmosenv.2009.12.013, 2010.

785 Seinfeld, J. H., and Pandis, S. N.: Atmospheric chemistry and physics: from air pollution to climate change,

786 John Wiley & Sons, Hoboken, NJ, 2016.

787 Shang, J., Passananti, M., Dupart, Y., Ciuraru, R., Tinel, L., Rossignol, S., Perrier, S., Zhu, T., and George,  
788 C.: SO<sub>2</sub> uptake on oleic acid: a new formation pathway of organosulfur compounds in the atmosphere, *Environ.*  
789 *Sci. Technol. Let.*, 3, 67-72, doi: 10.1021/acs.estlett.6b00006, 2016.

790 Shen, X. J., Sun, J. Y., Zhang, X. Y., Zhang, Y. M., Zhang, L., Che, H. C., Ma, Q. L., Yu, X. M., Yue, Y., and  
791 Zhang, Y. W.: Characterization of submicron aerosols and effect on visibility during a severe haze-fog episode in  
792 Yangtze River Delta, China, *Atmos. Environ.*, 120, 307-316, doi: 10.1016/j.atmosenv.2015.09.011, 2015.

793 Sipilä, M., Berndt, T., Petäjä, T., Brus, D., Vanhanen, J., Stratmann, F., Patokoski, J., Mauldin, R. L.,  
794 Hyvärinen, A.-P., Lihavainen, H., and Kulmala, M.: The role of sulfuric acid in atmospheric nucleation, *Science*,  
795 327, 1243-1246, doi: 10.1126/science.1180315, 2010.

796 Staudt, S., Kundu, S., Lehmler, H.-J., He, X., Cui, T., Lin, Y.-H., Kristensen, K., Glasius, M., Zhang, X.,  
797 Weber, R. J., Surratt, J. D., and Stone, E. A.: Aromatic organosulfates in atmospheric aerosols: synthesis,  
798 characterization, and abundance, *Atmos. Environ.*, 94, 366-373, doi: 10.1016/j.atmosenv.2014.05.049, 2014.

799 Sun, K., Tao, L., Miller, D. J., Pan, D., Golston, L. M., Zondlo, M. A., Griffin, R. J., Wallace, H. W., Leong,  
800 Y. J., Yang, M. M., Zhang, Y., Mauzerall, D. L., and Zhu, T.: Vehicle emissions as an important urban ammonia  
801 source in the United States and China, *Environ. Sci. Technol.*, 51, 2472-2481, doi: 10.1021/acs.est.6b02805, 2017.

802 Sun, Y., Chen, C., Zhang, Y., Xu, W., Zhou, L., Cheng, X., Zheng, H., Ji, D., Li, J., Tang, X., Fu, P., and  
803 Wang, Z.: Rapid formation and evolution of an extreme haze episode in Northern China during winter 2015, *Sci.*  
804 *Rep.*, 6, 27151, doi: 10.1038/srep27151, 2016.

805 Surratt, J. D., Kroll, J. H., Kleindienst, T. E., Edney, E. O., Claeys, M., Sorooshian, A., Ng, N. L., Offenberg,  
806 J. H., Lewandowski, M., Jaoui, M., Flagan, R. C., and Seinfeld, J. H.: Evidence for organosulfates in secondary  
807 organic aerosol, *Environ. Sci. Technol.*, 41, 517-527, doi: 10.1021/es062081q, 2007.

808 Takekawa, H., Minoura, H., and Yamazaki, S.: Temperature dependence of secondary organic aerosol  
809 formation by photo-oxidation of hydrocarbons, *Atmos. Environ.*, *37*, 3413-3424, doi: 10.1016/S1352-  
810 2310(03)00359-5, 2003.

811 Tan, J.-H., Duan, J.-C., Chen, D.-H., Wang, X.-H., Guo, S.-J., Bi, X.-H., Sheng, G.-Y., He, K.-B., and Fu, J.-  
812 M.: Chemical characteristics of haze during summer and winter in Guangzhou, *Atmos. Res.*, *94*, 238-245, doi:  
813 10.1016/j.atmosres.2009.05.016, 2009.

814 Tang, G., Sun, J., Wu, F., Sun, Y., Zhu, X., Geng, Y., and Wang, Y.: Organic composition of gasoline and its  
815 potential effects on air pollution in North China, *Sci. China Chem.*, *58*, 1416-1425, doi: 10.1007/s11426-015-  
816 5464-0, 2015.

817 Thalman, R., de Sá, S. S., Palm, B. B., Barbosa, H. M. J., Pöhlker, M. L., Alexander, M. L., Brito, J., Carbone,  
818 S., Castillo, P., Day, D. A., Kuang, C., Manzi, A., Ng, N. L., Sedlacek Iii, A. J., Souza, R., Springston, S., Watson,  
819 T., Pöhlker, C., Pöschl, U., Andreae, M. O., Artaxo, P., Jimenez, J. L., Martin, S. T., and Wang, J.: CCN activity  
820 and organic hygroscopicity of aerosols downwind of an urban region in central Amazonia: seasonal and diel  
821 variations and impact of anthropogenic emissions, *Atmos. Chem. Phys.*, *17*, 11779-11801, doi: 10.5194/acp-17-  
822 11779-2017, 2017.

823 Tkacik, D. S., Presto, A. A., Donahue, N. M., and Robinson, A. L.: Secondary organic aerosol formation  
824 from intermediate-volatility organic compounds: cyclic, linear, and branched alkanes, *Environ. Sci. Technol.*, *46*,  
825 8773-8781, doi: 10.1021/es301112c, 2012.

826 Tong, S., Hou, S., Zhang, Y., Chu, B., Liu, Y., He, H., Zhao, P., and Ge, M.: Exploring the nitrous acid  
827 (HONO) formation mechanism in winter Beijing: direct emissions and heterogeneous production in urban and  
828 suburban areas, *Faraday Discuss.*, *189*, 213-230, doi: 10.1039/c5fd00163c, 2016.

829 Ulbrich, I. M., Canagaratna, M. R., Zhang, Q., Worsnop, D. R., and Jimenez, J. L.: Interpretation of organic

830 components from positive matrix factorization of aerosol mass spectrometric data, *Atmos. Chem. Phys.*, 9, 2891-  
831 2918, doi: 10.5194/acp-9-2891-2009, 2009.

832 Wexler, A. S., and Clegg, S. L.: Atmospheric aerosol models for systems including the ions  $H^+$ ,  $NH_4^+$ ,  $Na^+$ ,  
833  $SO_4^{2-}$ ,  $NO_3^-$ ,  $Cl^-$ ,  $Br^-$ , and  $H_2O$ , *J. Geophys. Res.-Atmos.*, 107, doi: 10.1029/2001jd000451, 2002.

834 Xu, J., Huang, M.-Q., Cai, S.-Y., Liao, Y.-M., Hu, C.-J., Zhao, W.-X., Gu, X.-J., and Zhang, W.-J.: Chemical  
835 composition and reaction mechanisms for aged p-xylene secondary organic aerosol in the presence of ammonia,  
836 *J. Chin. Chem. Soc-taipei*, 65, 578-590, doi: 10.1002/jccs.201700249, 2018.

837 Yang, S., Yuesi, W., and Changchun, Z.: Measurement of the vertical profile of atmospheric  $SO_2$  during the  
838 heating period in Beijing on days of high air pollution, *Atmos. Environ.*, 43, 468-472, doi:  
839 10.1016/j.atmosenv.2008.09.057, 2009.

840 Yang, W., Li, J., Wang, M., Sun, Y., and Wang, Z.: A case study of investigating secondary organic aerosol  
841 formation pathways in Beijing using an observation-based SOA Box Model, *Aerosol Air Qual. Res.*, 18, 1606-  
842 1616, doi: 10.4209/aaqr.2017.10.0415, 2018.

843 Ye, P., Ding, X., Hakala, J., Hofbauer, V., Robinson, E. S., and Donahue, N. M.: Vapor wall loss of semi-  
844 volatile organic compounds in a Teflon chamber, *Aerosol Sci. Tech.*, 50, 822-834, doi:  
845 10.1080/02786826.2016.1195905, 2016.

846 Yuan, B., Koss, A. R., Warneke, C., Coggon, M., Sekimoto, K., and de Gouw, J. A.: Proton-transfer-reaction  
847 mass spectrometry: Applications in atmospheric sciences, *Chem. Rev.*, 117, 13187-13229, doi:  
848 10.1021/acs.chemrev.7b00325, 2017.

849 Zhang, L., Chen, Y., Zhao, Y., Henze, D. K., Zhu, L., Song, Y., Paulot, F., Liu, X., Pan, Y., Lin, Y., and Huang,  
850 B.: Agricultural ammonia emissions in China: reconciling bottom-up and top-down estimates, *Atmos. Chem.*  
851 *Phys.*, 18, 339-355, doi: 10.5194/acp-18-339-2018, 2018.



852 Zhang, Q., Streets, D. G., He, K., and Klimont, Z.: Major components of China's anthropogenic primary  
853 particulate emissions, *Environ. Res. Lett.*, 2, doi: 10.1088/1748-9326/2/4/045027, 2007.

854 Zhang, X., Cappa, C. D., Jathar, S. H., McVay, R. C., Ensberg, J. J., Kleeman, M. J., and Seinfeld, J. H.:  
855 Influence of vapor wall loss in laboratory chambers on yields of secondary organic aerosol, *Proc. Natl. Acad. Sci.*  
856 USA, 111, 5802-5807, doi: 10.1073/pnas.1404727111, 2014.

857 Zhang, X., Schwantes, R. H., McVay, R. C., Lignell, H., Coggon, M. M., Flagan, R. C., and Seinfeld, J. H.:  
858 Vapor wall deposition in Teflon chambers, *Atmos. Chem. Phys.*, 15, 4197-4214, doi: 10.5194/acp-15-4197-2015,  
859 2015.

860 Zhang, Y., Wang, X., Zhang, Z., Lü, S., Shao, M., Lee, F. S. C., and Yu, J.: Species profiles and normalized  
861 reactivity of volatile organic compounds from gasoline evaporation in China, *Atmos. Environ.*, 79, 110-118, doi:  
862 10.1016/j.atmosenv.2013.06.029, 2013.

863 Zhao, B., Wang, S., Donahue, N. M., Jathar, S. H., Huang, X., Wu, W., Hao, J., and Robinson, A. L.:  
864 Quantifying the effect of organic aerosol aging and intermediate-volatility emissions on regional-scale aerosol  
865 pollution in China, *Sci. Rep.*, 6, doi: 10.1038/srep28815, 2016.

866 Zhao, D., Schmitt, S. H., Wang, M., Acir, I. H., Tillmann, R., Tan, Z., Novelli, A., Fuchs, H., Pullinen, I.,  
867 Wegener, R., Rohrer, F., Wildt, J., Kiendler-Scharr, A., Wahner, A., and Mentel, T. F.: Effects of NO<sub>x</sub> and SO<sub>2</sub> on  
868 the secondary organic aerosol formation from photooxidation of  $\alpha$ -pinene and limonene, *Atmos. Chem. Phys.*, 18,  
869 1611-1628, doi: 10.5194/acp-18-1611-2018, 2018.

870 Zhao, D., Song, X., Zhu, T., Zhang, Z., Liu, Y., and Shang, J.: Multiphase oxidation of SO<sub>2</sub> by NO<sub>2</sub> on CaCO<sub>3</sub>  
871 particles, *Atmos. Chem. Phys.*, 18, 2481-2493, doi: 10.5194/acp-18-2481-2018, 2018.

872 Zheng, B., Zhang, Q., Zhang, Y., He, K. B., Wang, K., Zheng, G. J., Duan, F. K., Ma, Y. L., and Kimoto, T.:  
873 Heterogeneous chemistry: a mechanism missing in current models to explain secondary inorganic aerosol

874 formation during the January 2013 haze episode in North China, *Atmos. Chem. Phys.*, 15, 2031-2049, doi:  
875 10.5194/acp-15-2031-2015, 2015.

876 Zou, Y., Deng, X. J., Zhu, D., Gong, D. C., Wang, H., Li, F., Tan, H. B., Deng, T., Mai, B. R., Liu, X. T., and  
877 Wang, B. G.: Characteristics of 1 year of observational data of VOCs, NO<sub>x</sub> and O<sub>3</sub> at a suburban site in Guangzhou,  
878 China, *Atmos. Chem. Phys.*, 15, 6625-6636, doi: 10.5194/acp-15-6625-2015, 2015.

Table 1. Summary of experimental conditions in this study.

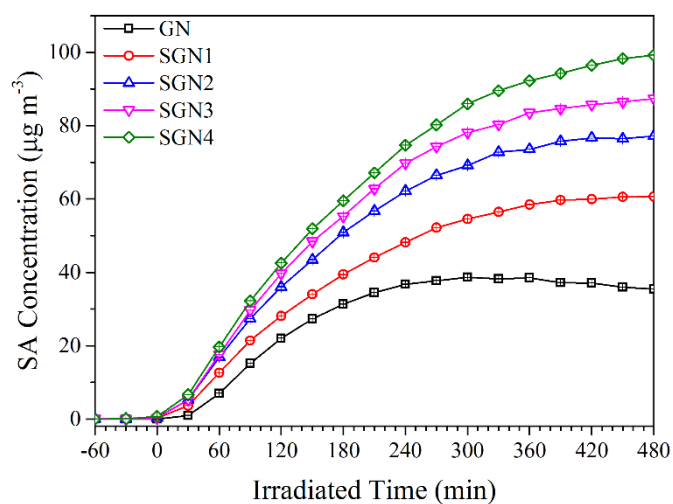
Exp. <sup>a</sup>	RH (%)	T (°C)	SO <sub>2</sub> (ppb)	NH <sub>3</sub> <sup>b</sup> (ppb)	HC <sub>0</sub> (ppb)	NO <sub>x,0</sub> (ppb)	HC <sub>0</sub> /NO <sub>x,0</sub> (ppbC ppb <sup>-1</sup> )	Surface <sup>c</sup> (μm <sup>2</sup> cm <sup>-3</sup> )	ΔHC (μg m <sup>-3</sup> )	ΔM (μg m <sup>-3</sup> )	SA yield <sup>d</sup>
GN	50±3	26±1	–	–	411.0	128.4	20.61	1.12×10 <sup>3</sup>	747.8	34.6	0.130
SGN1	50±3	26±1	35	–	419.8	121.0	22.34	1.73×10 <sup>3</sup>	871.6	58.0	0.155
SGN2	50±3	26±1	74	–	412.0	121.3	21.88	2.06×10 <sup>3</sup>	866.2	77.8	0.193
SGN3	50±3	26±1	116	–	383.6	119.8	20.62	2.23×10 <sup>3</sup>	791.1	87.1	0.226
SGN4	50±3	26±1	151	–	394.4	125.9	20.17	2.46×10 <sup>3</sup>	810.7	106.3	0.258
AGN1	50±3	26±1	–	150	413.8	120.4	22.12	1.79×10 <sup>3</sup>	700.6	47.6	0.158
AGN2	50±3	26±1	–	200	411.5	122.6	21.61	2.23×10 <sup>3</sup>	749.1	58.3	0.166

880 <sup>a</sup> Letters in abbreviations represent the reactants introduced into the chamber reactor, i.e., “G” represents  
 881 gasoline, “N” represents nitrogen oxides, “S” represents sulfur dioxide, “A” represents ammonia.

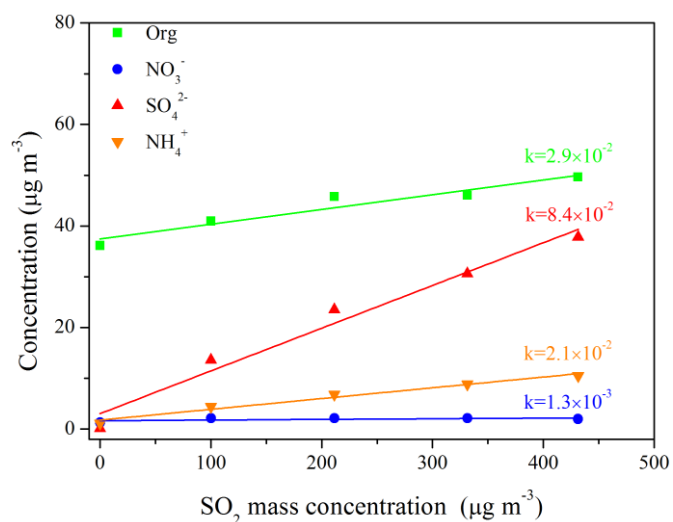
882 <sup>b</sup> The concentration of NH<sub>3</sub> is estimated by the amount of NH<sub>3</sub> added and the volume of the smog chamber.

883 <sup>c</sup> The surface area of aerosol particles measured by SMPS after 480 min of each experiment.

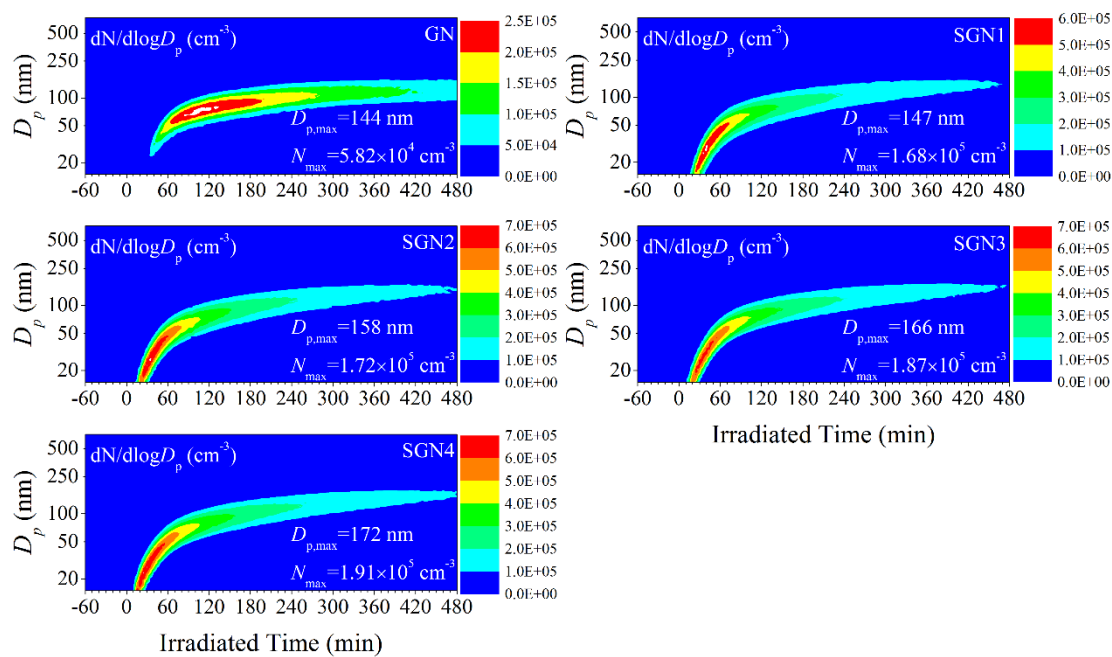
884 <sup>d</sup> SA yield was calculated after taking vapor and particle wall loss into account.



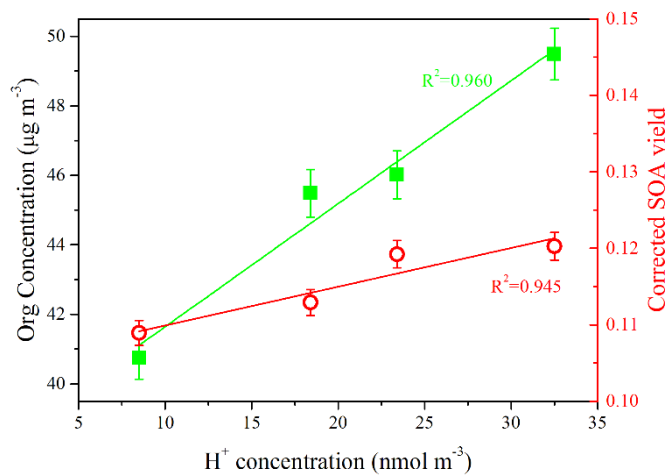
885  
 886 Fig. 1. Time series of secondary aerosol concentrations during the photo-oxidation experiments with different SO<sub>2</sub>  
 887 concentrations (Exps. GN, SGN1, SGN2, SGN3, and SGN4).



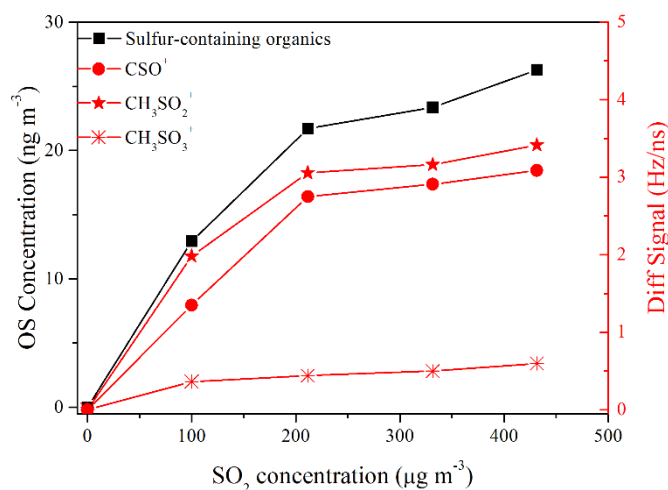
888  
 889 Fig. 2. Linear relationship between the concentration of chemical species (i.e., organic (green), nitrate (blue), sulfate (red), and  
 890 ammonium (orange)) and SO<sub>2</sub> under different SO<sub>2</sub> initial concentration conditions (Exps. GN, SGN1, SGN2, SGN3, and  
 891 SGN4). Each line represents a linear fitting and the k values are the corresponding slopes for each chemical species.



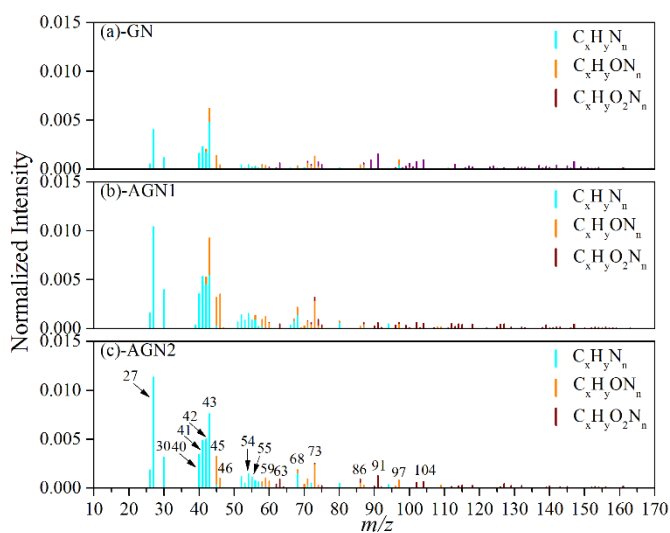
892  
 893 Fig. 3. Time series of the size distributions for the generated secondary aerosol during the photo-oxidation experiments with  
 894 different SO<sub>2</sub> initial concentrations (Exps. GN, SGN1, SGN2, SGN3, and SGN4).  $D_{p,max}$  and  $N_{max}$  represent the maximal  
 895 diameter and number concentration of generated secondary aerosol, respectively, during each photo-oxidation experiment.



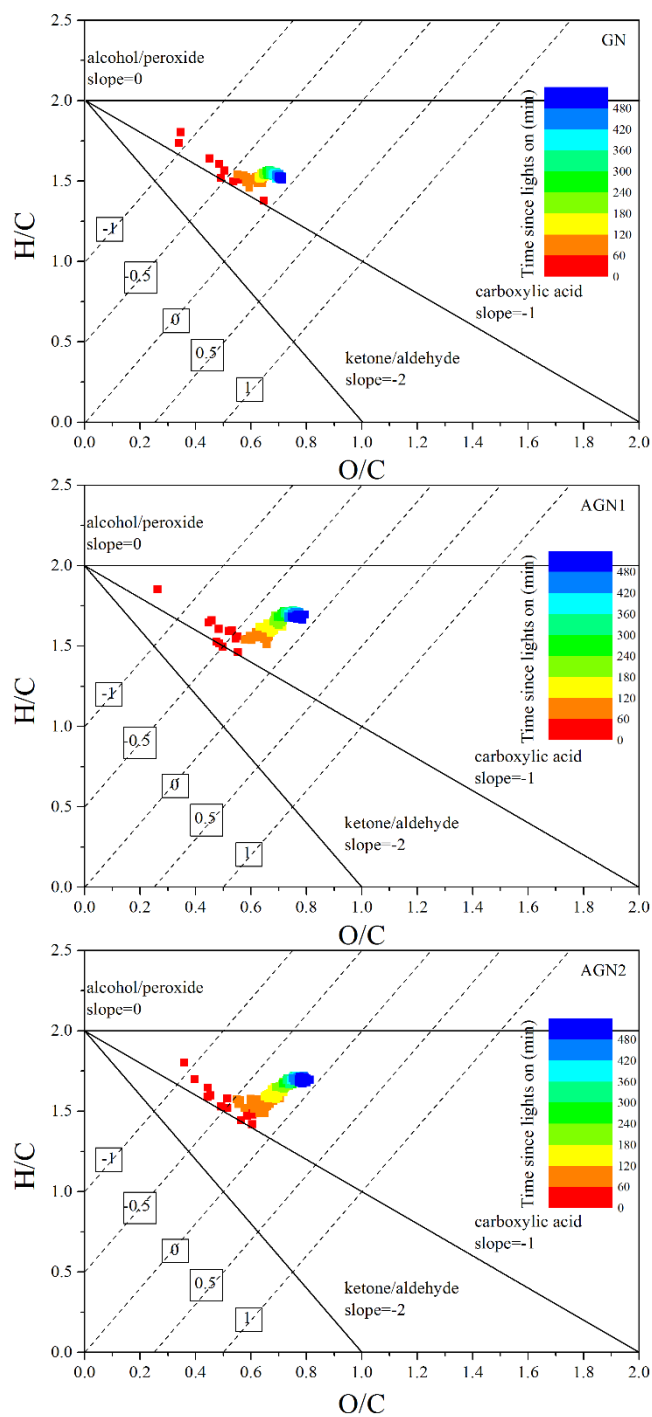
896  
 897 Fig. 4. Relationship between SOA concentration (left y axis), corrected SOA yield (right y axis) and H<sup>+</sup> concentration, which  
 898 was used to characterize the particle acidities. The H<sup>+</sup> concentration presented in this plot was the value when the SOA  
 899 formation rate reached the peak during each experiment (Exps. SGN1, SGN2, SGN3, and SGN4).



900  
 901 Fig. 5. Signal of fitted peaks, i.e., CSO<sup>+</sup>, CH<sub>3</sub>SO<sub>2</sub><sup>+</sup>, CH<sub>3</sub>SO<sub>3</sub><sup>+</sup> (right y axis) and sulfur-containing organics concentration (left  
 902 y axis) as a function of SO<sub>2</sub> initial concentration.



903  
 904 Fig. 6. Typical normalized mass spectra of N-containing fragments in SOA formed from the photo-oxidation of gasoline vapor  
 905 at different concentrations of NH<sub>3</sub> (Exps. GN, AGN1 and AGN2).



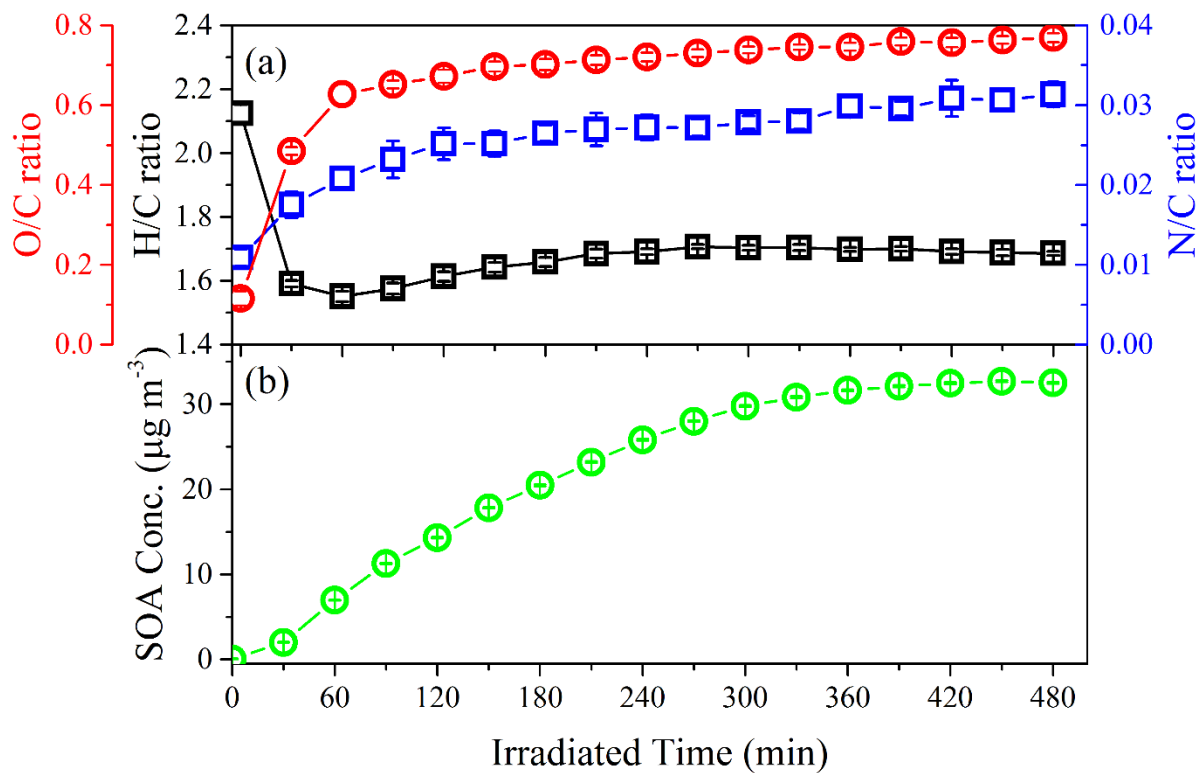
906

907 Fig. 7. Time evolution of H/C and O/C in SOA formed from the photo-oxidation of gasoline vapor at different concentrations

908 of  $\text{NH}_3$  (Exp. GN, AGN1 and AGN2). The numbers (i.e., -1, -0.5, 0, 0.5, and 1) labeling the dashed lines show the average

909 carbon oxidation state ( $\text{OSc} = 2 \times \text{O/C} - \text{H/C}$ ) (Kroll et al., 2011). The black lines represent the addition of functional groups

910 to an aliphatic carbon (Heald et al., 2010).

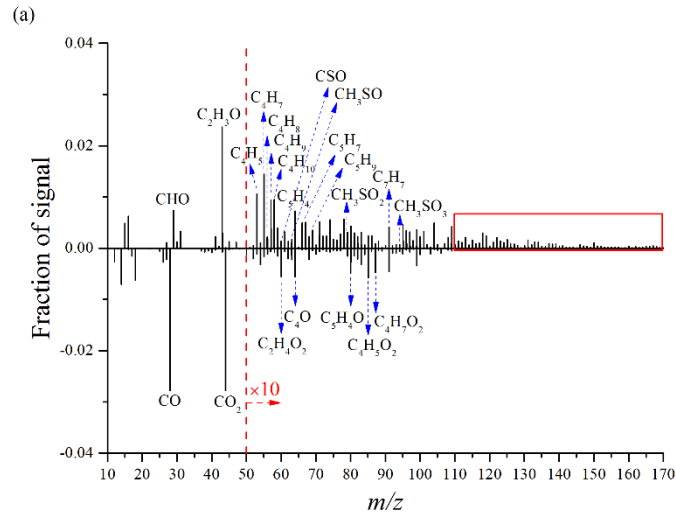


911

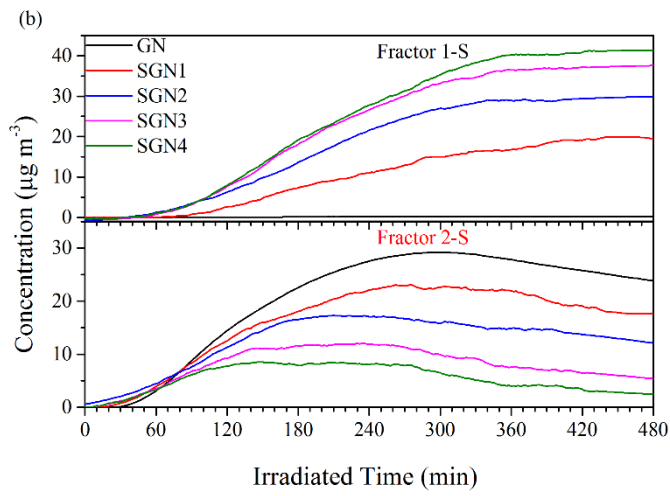
912 Fig. 8. Time evolution of (a) O/C, H/C and N/C and (b) SOA concentration in the photo-oxidation of gasoline vapor in the

913 presence of 150 ppb  $\text{NH}_3$  (Exp. AGN1).

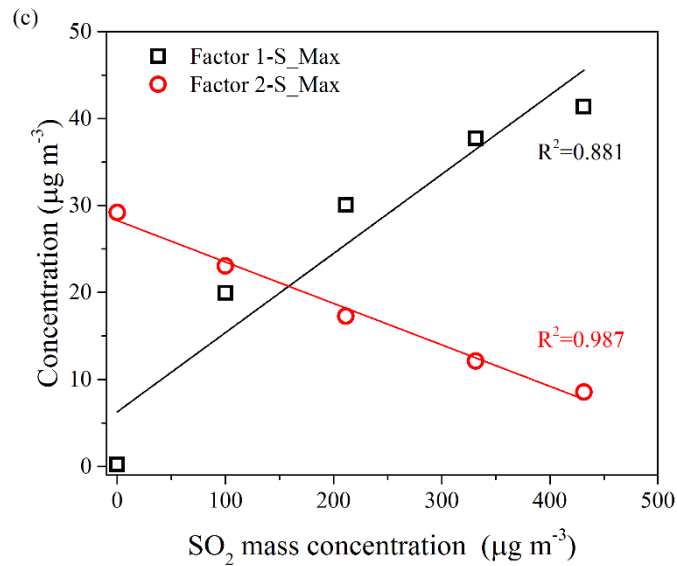




914



915



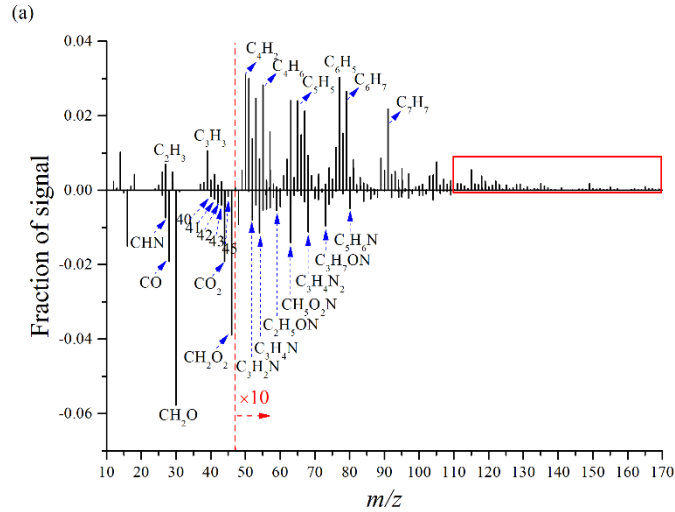
916

917 Fig. 9. (a) Difference mass spectra (Factor 1-S–Factor 2-S) between the two factors, (b) Time series of the mass concentration,

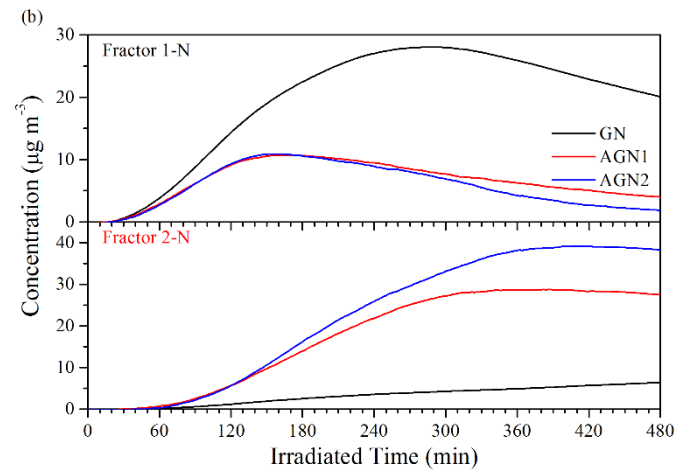
918 and (c) Relationship between the concentration of SO<sub>2</sub> and the maximum concentration of the two factors identified by

919 applying PMF analysis to the AMS data derived from the experiments at different concentrations of SO<sub>2</sub> (Exps. GN, SGN1,

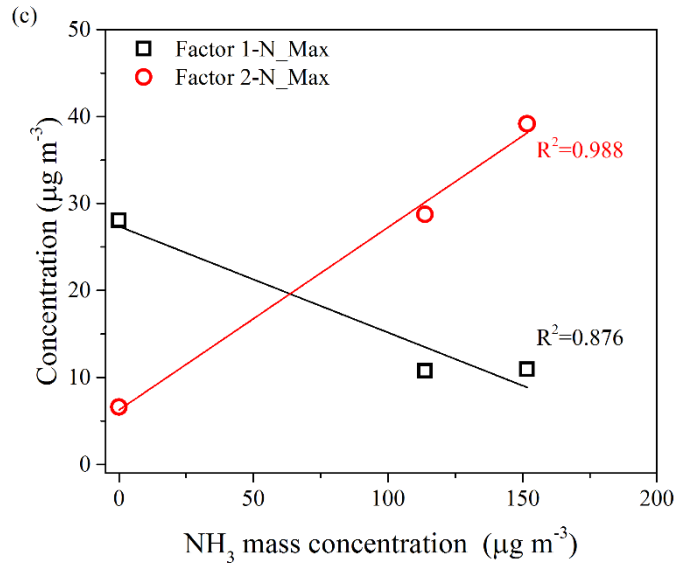
920 SGN2, SGN3 and SGN4).



921



922



923

924 Fig. 10. (a) Difference mass spectra (Factor 1-N–Factor 2-N) between the two factors, (b) Time series of the mass

925 concentration, and (c) Relationship between the concentration of  $\text{NH}_3$  and the maximum concentration of the two

926 factors identified by applying PMF analysis to the AMS data derived from the experiments at different

927 concentrations of  $\text{NH}_3$  (Exps. GN, AGN1 and AGN2).